WADC TECHNICAL REPORT 59-574

BEHAVIOR OF PLASTIC MATERIALS IN HYPERTHERMAL ENVIRONMENTS

Donald L. Schmidt

Materials Laboratory

APRIL 1960

WRIGHT AIR DEVELOPMENT CENTER

WADC TECHNICAL REPORT 59-574

BEHAVIOR OF PLASTIC MATERIALS IN HYPERTHERMAL ENVIRONMENTS

Donald L. Schmidt

Materials Laboratory

April 1960

Project No. 7340

= USAF

WRIGHT AIR DEVELOPMENT CENTER
AIR RESEARCH AND DEVELOPMENT COMMAND
UNITED STATES AIR FORCE
WRIGHT-PATTERSON AIR FORCE BASE, OHIO

400 – March 1960 – 26-746

FOREWORD

This report was prepared by the Non-Metallic Materials Division. The work was initiated under Project No. 7340, "Non-Metallic and Composite Materials," Task No. 73400, "Organic and Inorganic Plastics." It was administered under the direction of the Materials Laboratory, Directorate of Laboratories, Wright Air Development Center, with Mr. Donald L. Schmidt acting as project engineer.

The materials investigated were not necessarily formulated to withstand the environments to which they were exposed in this program and, therefore, their performance as reported herein should in no way reflect on their performance under less severe conditions. This report covers work conducted from January 1959 to May 1959.

The author wishes to acknowledge with appreciation the valuable discussions and suggestions of Messrs. H. Schwartz and R. Farmer of the Materials Laboratory, WADC, which contributed greatly in the preparation of this report.

ABSTRACT

A systematic investigation of the behavior of plastic materials in very high temperature air is reported. Several test models of various compositions and constructions were exposed in the air plasma of a one megawatt stabilized electric arc. Both descriptive and quantitative data were obtained on the characteristics and physical properties of the ablative materials.

A thermal analysis of quasi steady-state ablation at the stagnation point of the test models was performed. Individual heat transfer parameters were numerically estimated for the plastic materials and test conditions under consideration.

PUBLICATION REVIEW

This report has been reviewed and is approved.

FOR THE COMMANDER:

R. T. Schwartz

R. T. SCHWARTZ
Chief, Nonmetallic Materials Laboratory
Materials Central

TABLE OF CONTENTS

LIST OF ILLUSTRATIONS

LIST OF ILLUSTRATIONS (Cont'd.)

LIST OF TABLES

SECTION I

INTRODUCTION

Aerothermochemical problems of hypersonic flight in the atmospheric medium are a serious impediment in the design of high performance vehicles. Gas temperatures and aerodynamic heating rates encountered by these vehicles are generally of an extreme nature, especially when a high velocity is allowed to persist in the lower atmospheric regions. Under such conditions, stagnation temperatures may exceed the melting, vaporization or sublimination temperature of all known structural materials. In addition, the incident heat transferred to the surface of the vehicle may exceed its heat capacity and cause a destructive phase change in the material. In order to circumvent this thermal barrier problem, it often becomes necessary to use unique thermal protective materials on the vehicle.

Essentially three materials systems have been investigated as means for thermally protecting hypersonic vehicles during transient flight in the atmosphere. These materials systems are based on heat sink, internal cooling, or mass transfer cooling (ablation, transpiration cooling, and fluid addition) processes to absorb and dissipate the incident aerodynamic heat flux (1). Heat sink materials absorb thermal energy sensibly through a temperature rise, but without an accompanying phase change. Internal cooling systems absorb the incident heat flux through a thin wall and transfer it to a coolant, which may or may not undergo a phase change. In mass transfer cooling systems, heat is absorbed and dissipated principally by gas or fluid injection into the adjacent boundary layer. Characteristics of the boundary layer are altered by the presence of the foreign matter, and the incident flux is thereby reduced to an acceptable level.

Heat sink materials have been successfully used for the thermal protection of ballistic re-entry vehicles. Aerodynamic heating of these re-entry bodies had to be limited by blunt high-drag design, because of the limited thermal capacity of the heat-shielding metallic material. In the future, re-entry vehicles will travel through the atmosphere at higher speeds and encounter significantly greater aerodynamic heating. Consequently, the blunt body-heat sink concept of thermal protection will not be usable in these hypervelocity vehicles. Internal cooling, transpiration cooling, and fluid addition systems offer considerably more promise in this respect, but past experiences have revealed great difficulties in applying these systems to actual hardware items. On the contrary, ablative material

---

Manuscript released by the author 1 August 1959 for publication as a WADC Technical Report.

systems provide a simple and powerful means for protecting vehicles over a wide range of incident thermal fluxes. This unique behavior is due to the automatic heat shielding mechanism and surface temperature control which is brought about by sacrificial loss of mass.

The concept of re-entry thermal shielding with ablative materials has been experimentally verified in the laboratory and proven in actual flight testing. Reinforced plastics, as one class of ablative materials, have received considerable attention by virtue of their superior high temperature performance as compared to other classes of conventional high temperature materials (2,3). The unique combination of heat dissipative, thermal and structural properties of plastics are excellent for protecting missile components from aerodynamic heating.

Although the re-entry heating problem has been solved for certain re-entry vehicles, the search continues for new and improved ablative materials. Each new re-entry design brings forth a new aerothermochemical flight environment, depending upon the vehicle speed, configuration and boundary layer conditions. Ablative plastics which have proven successful in past re-entry environments may not be optimum, nor even usable in future designs. Furthermore, the current state-of-the-art of ablative materials does not permit a detailed and accurate prediction of performance for new design environments. This is due to the limited theory and experimental data available on ablative materials. The need is apparent, then, for determining the characteristics and performance of plastic materials in a wide range and combination of laboratory generated hyperthermal environments to obtain data suitable for analyses and subsequent formulation of suitable hypotheses which will form the basis for additional materials research (4).

For the past several years, the Materials Laboratory, WADC, has been conducting systematic investigations on ablative plastic materials. The purposes of these studies were to (a) gain a better insight into the ablative processes and associated thermal protective mechanisms, (b) obtain descriptive and experimental data on available and improved ablative materials over a wide range and combination of hyperthermal environments, (c) develop analytical solutions to furnish guidance in predicting materials performance in new design environments and, (d) develop applicable theories and identify trends useful in the further improvement of plastic ablative materials. Fundamental and engineering aspects of ablation have been emphasized in preference to obtaining design type data for specific applications.

The purpose of this report is to record a phase of the above discussed materials research program. The report shall be limited to the ablative characteristics and physical properties of three reinforced plastic materials in a high temperature air plasma environment.

All symbols used in this report, and their units of value are defined in Appendix I.

SECTION II

ABLATION OF PLASTIC MATERIALS

Reinforced plastic materials withstand extremely high temperatures for transitory periods due to the ability to absorb and dissipate heat. During exposure, the materials undergo combined thermal-chemical-mechanical degradation with an attendant removal of surface material. This phenomena, commonly known as ablation, thermally shields the material from the environment and provides for an automatic temperature control of the exposed surface.

Ablation comprises three salient mechanisms of heat absorption and dissipation. They are (a) absorption of heat by endothermic chemical reactions and thermodynamic changes of state, (b) reduced convective heat transfer to the surface of the body by mass injection of pyrolytic gases into the boundary layer and (c) radiant emission from the high temperature ablating surface. Each of these thermal protective mechanisms depend upon a large number of environmental and materials parameters. The magnitude of these effects has been presented analytically, but considerable experimental work is required for confirmation.

Figure 1 is a schematic illustration of the behavior of a reinforced plastic material during ablation. High temperatures of the gas stream are restricted to the surface region of the body by the low thermal conductivity of the material. Limited penetration of heat into the substrate material promotes higher surface temperatures which may (a) increase radiant emission from the body, (b) increase volatilization of molten liquid (if present) from the surface and (c) provide for a closer approach to thermal equilibrium conditions. In the surface region, the material absorbs heat as its temperature is raised sensibly to a point approaching various phase changes. Depolymerization, fusion, vaporization and sublimation processes may then occur with additional absorption of heat from the surroundings. Organic components in the ablating material are pyrolyzed into residual carbonaceous material and large volumes of gaseous products. These gases are injected into the boundary layer and envelop the surfaces of the model in a layer of relatively "cool gases." Temperature and velocity profiles in the boundary layer are distorted, which produce an associated reduction in both convective heat transfer and aerodynamic shear. Inorganic components, if present, undergo melting and partial vaporization. A fraction of this molten material is retained on the surface as a molten film or beads. The remainder of the liquid flows along the body in the direction of the gas stream and transfers heat away from the stagnation region. The amount of material vaporized or mechanically removed in the liquid state is dependent upon the enthalpy gradient in the boundary layer, viscosity of the melt, and shear forces acting at the gas-liquid interface.

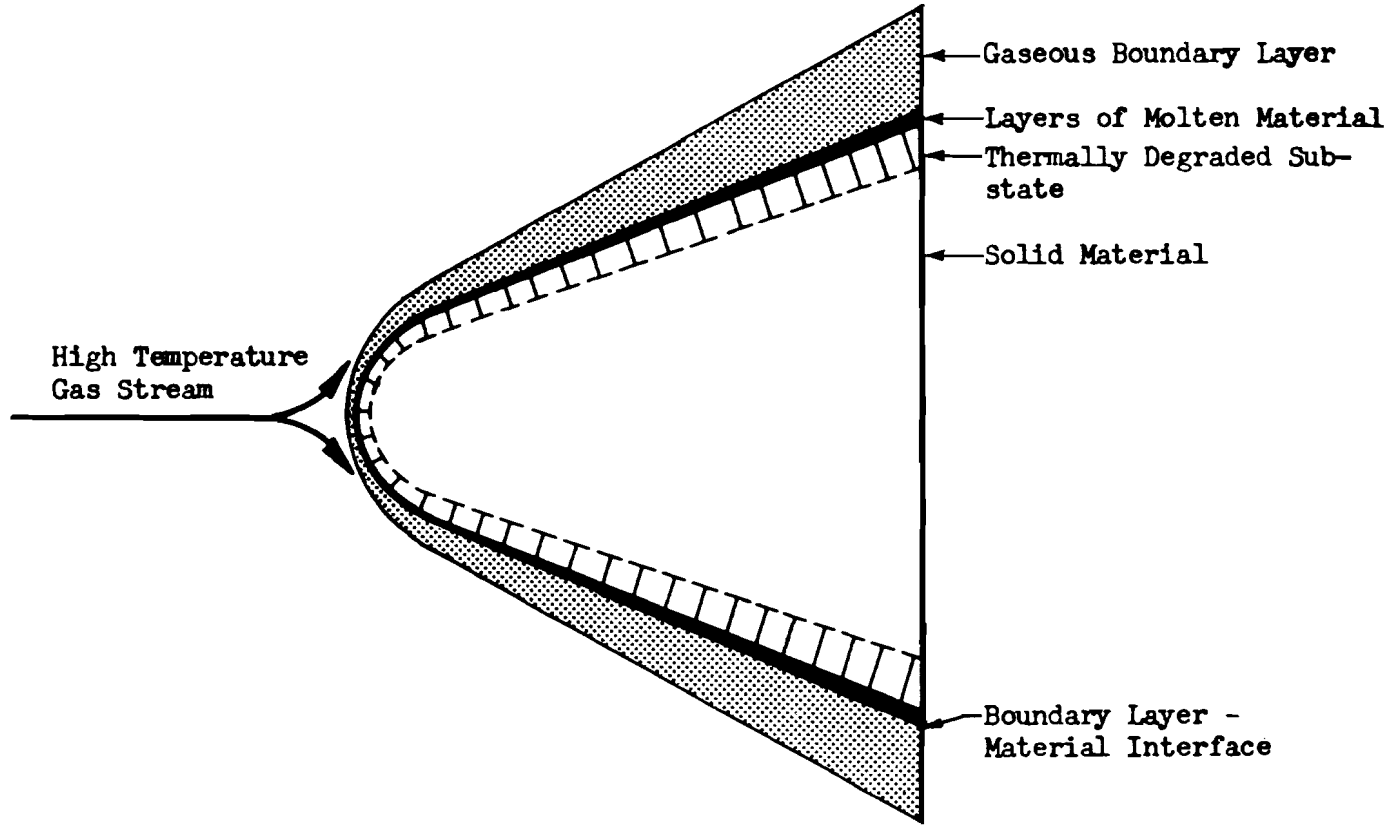

Figure 1. Reinforced Plastic Material Undergoing Ablation

SECTION III

MATERIALS INVESTIGATED

Materials

Three reinforced organic plastics in a laminar or molded construction were evaluated. The laminar sample was composed of parallel layers of nylon fabric impregnated with 33 percent phenolic resin, and identified by a Materials Laboratory code number of Y-31. The second sample, Y-32, was molded with one-half inch squares of nylon fabric impregnated with 53 percent phenolic resin. A third sample, designated Y-33, was molded from one-half inch nylon squares impregnated with 50 percent melamine resin.

A complete description of the composition, construction, and method of specimen fabrication as furnished by the fabricators is given in Appendix II.

Test Specimens

One conical test model was machined from each of the submitted samples in accordance with the standard specimen configuration shown in Figure 2. A large specimen was selected for these studies to facilitate the acquisition of realistic and meaningful data, and to reduce model scaling effects. Another reason for using a large size model was to minimize component orientation effects, which may be unfavorable.

No attempt was made to use a scaled-down model of an actual nose cone design. The model configuration was selected on the basis of obtaining uniform heating and plasma flow at the stagnation point. The same specimen configuration was used for all models.

Quality Assurance

Each specimen was non-destructively inspected using X-ray analysis. A detailed visual inspection of the X-ray negatives failed to show any large internal defects in the specimens, such as voids, inclusions or delaminations. No surface defects were detected on the Y-31 and Y-32 models. Several hairline cracks were noted on the Y-33 specimen, and these minor defects were presumably due to a non-optimum molding cycle. Chopped nylon fabric was used in the molded specimens to give a randomly oriented reinforcement. However, the fabric squares aligned predominantly in a plane parallel to the base of the specimen.

On the basis of the above inspection data, the three test models were adjudged acceptable for evaluation purposes.

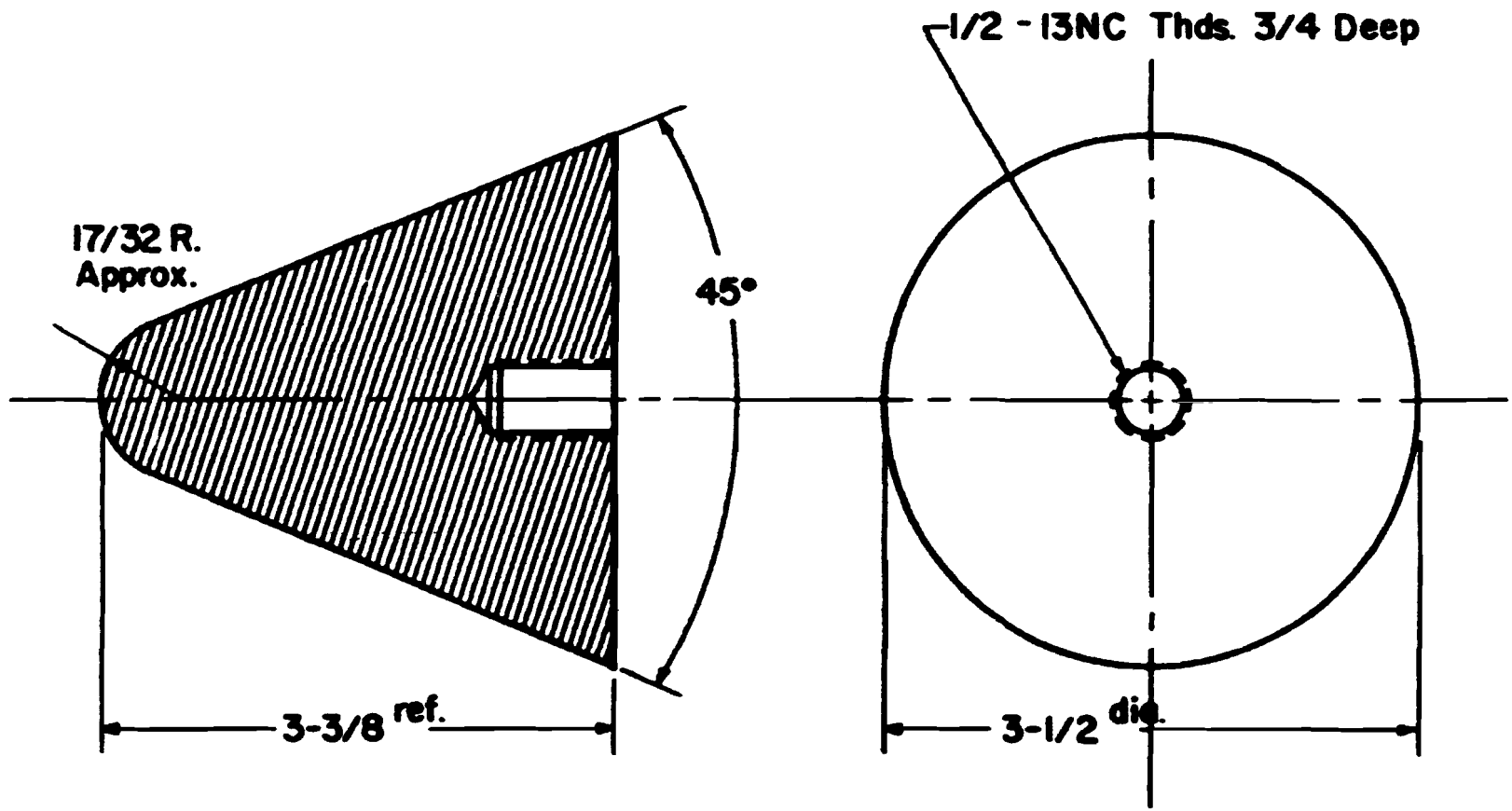

Figure 2. Standard Sample Shape

SECTION IV

EVALUATION FACILITY

An air plasma generator was used in the investigation to create the desired high temperature air environment. The unit was basically a one megawatt, air-stabilized electric arc with associated equipment, which is shown in Figure 3. It was designed, constructed, calibrated and operated by the University of Chicago, Chicago Midway Laboratories under Air Force Contract AF 33(616)-5436.

The stabilized electric arc unit was composed of a water-cooled chamber, a one and one-half inch diameter rod-shaped graphite anode, and a disc-shaped graphite cathode containing a one and one-quarter inch diameter centrally located orifice. The anode was movable, and controlled manually or hydraulically to maintain constant current operation in the arc unit. Both electrodes were contained within the arc chamber.

The unit was operated by first admitting high pressure air to the chamber to provide a stable swirling gas column within the chamber. The electric arc was then established between the electrodes and stabilized within the vortex of the air column. Pressure differential between the arc chamber and the exhaust atmosphere forced the plasma stream through the cathode orifice and into the exposure site.

Environmental parameters of the air plasma stream were measured at the exposure site and in the vicinity of the specimen apex. Temperatures were determined spectroscopically using oxygen and nitrogen spectral lines and molecular band spectra. Initial heat transfer rates to the models were measured with several copper calorimeters. Flux values were computed for the model apex region from well known heat transfer equations, based on one-dimensional heat transfer and time-to-melt relations. The velocity of the air plasma stream was determined by photographically measuring the position of foreign particles in the jet as a function of time. The free stream enthalpy was estimated from an energy balance of the system, based on a knowledge of the electrical energy input to the arc unit and associated heat losses to the electrodes, chamber and similar factors.

The characteristics of the plasma jet in the vicinity of the specimen apex, i.e. 4.5 inches above the cathode, were determined to be:

Temperature	8,000° to 9,000°K
Cold-wall heat flux	1,950 Btu/ft^2-sec
Gas velocity	2,500 ft/sec
Enthalpy	9,000 Btu/lb

for arc operating conditions of:

Current	3,500 amperes
Voltage	300 volts
Mass-flow	0.25 lb/sec

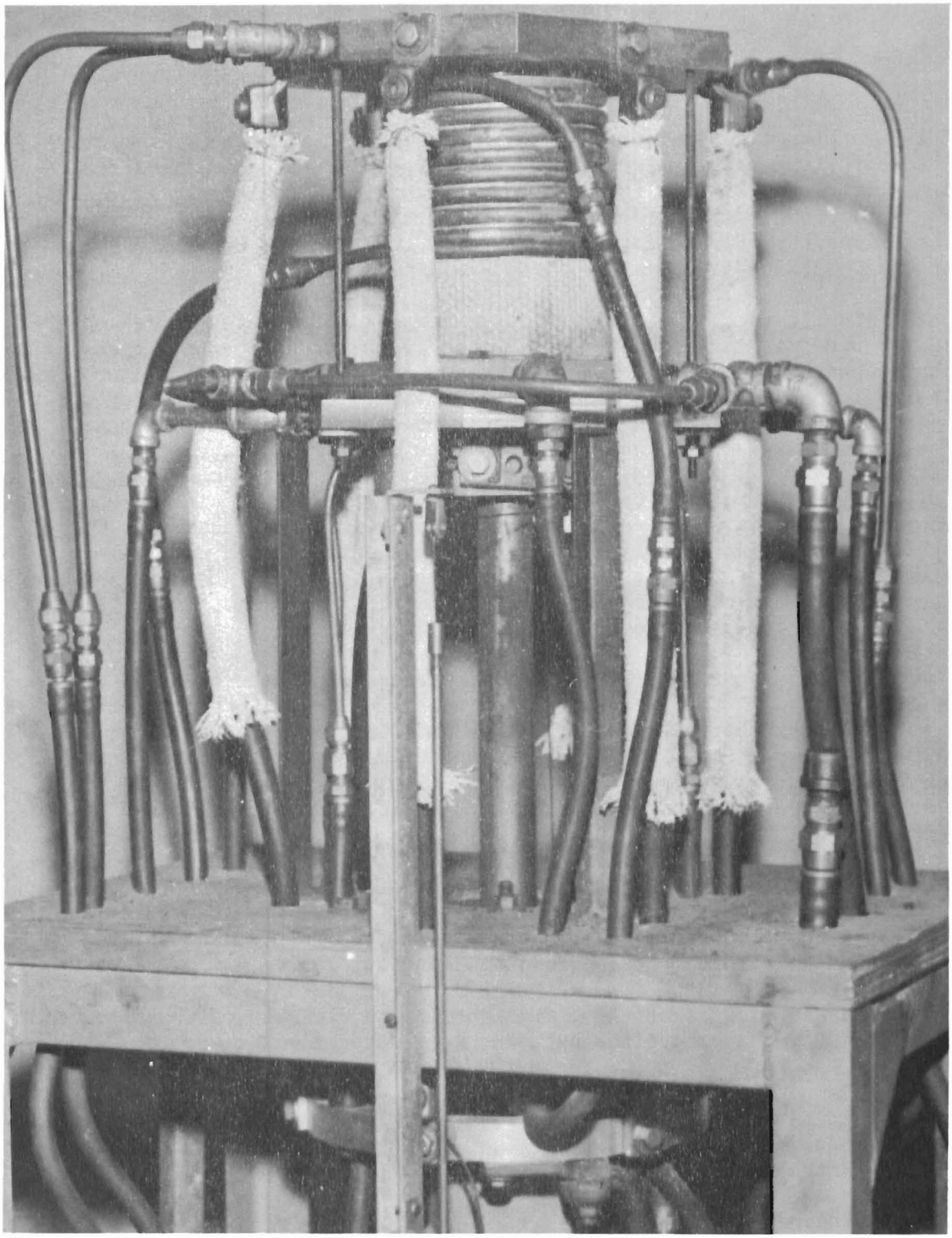

Figure 3. One Megawatt Air-Stabilized Plasma Arc Generator

A detailed description of the operation and characteristics of the air plasma generator are given in reference (5).

SECTION V

SPECIMEN EXPOSURE

The conical test model was mounted on a threaded graphite holder about 22 inches above the cathode, and protected from the plasma stream with a V-shaped transite shield. After the arc was brought to the desired operating conditions and stabilized, the protected specimen and shield were lowered to the proper position. The shield was then withdrawn rapidly and exposure commenced. At the same time, a high speed camera focused on the test specimen was actuated. The exposure period was continued for approximately 30 seconds, which was sufficient to establish quasi steady-state ablation without total destruction of the model. The exposure period was terminated by shutting off the power to the arc. The air supply to the arc chamber was maintained, however, to rapidly cool the chamber walls, electrodes and exposed specimen. The specimen was then removed from the holder for subsequent observation and physical measurements.

SECTION VI

TEST PROCEDURES

Descriptive and experimental data were obtained on the test ablative materials using the following evaluation procedures.

External Appearance

Model performance during ablation was permanently recorded using color motion photography. Specimens immersed in the high temperature plasma stream were observed with a 16mm movie camera at a rate of 32 frames per second. The camera was fitted with a lens filter to reduce the light intensity of the plasma stream, and thereby permit observation of the model.

General materials response to the environment was determined from careful observation and study of the motion picture film. Surface effects, profile changes, and boundary layer thickening during ablation were readily apparent.

Boundary Layer

Thickening of the boundary layer during ablation was readily observed with the aid of color motion pictures. The volume of gaseous products involved in boundary layer thickening could not be measured, but an

indication of this value was deduced from the mass ablation rate and the apparent thickness of the gaseous envelope surrounding the model.

Profile Changes

Two-dimensional profile changes of the models during exposure were recorded with color motion pictures. Original and post-exposure profiles of the models were also recorded by black-and-white silhouette photographs.

Surface Temperatures

No attempt was made to experimentally measure the surface temperature of the ablating models. A good approximation of the surface temperature was obtained from the work of other investigators on identical materials in similar plasma arc environments (5).

Stagnation Point Linear Ablation

The velocity of recession of the model apex was measured from the color motion picture film. A film comparator was used to obtain the surface displacement at intervals of one second exposure. Data were plotted for stagnation point linear ablation as a function of exposure time.

The instantaneous rate of linear ablation at the specimen apex was determined by measuring the slope of the line from a plot of linear erosion versus time.

The time to establish quasi steady-state ablation was also determined from the plot of stagnation point linear ablation versus time.

Mass Ablation

Total mass ablation was determined by weighing the test models before and immediately after exposure. Carbonized surface material was then removed from the models, and the specimens reweighed. These data along with a knowledge of the exposure period permitted the average rate of mass ablation to be calculated.

The stagnation point mass ablation rate $\dot{m}$ was determined from linear ablation measurements. The value was computed as the sum of material physically removed by thermal-chemical-mechanical factors and volatilization losses from the char layer, expressed on a unit time basis. The following relation was used:

$$\dot{m} = \frac{x_l \rho_b + x_c(\rho_b - \rho_c)}{T} \quad . \tag{1}$$

Where:

x_l = total linear erosion
x_c = depth of major heat penetration into substrate, i.e. post-exposure char layer thickness

ρ_b = density of solid body
ρ_c = density of char layer
T = unit of time.

Volatilization losses from the thin damaged zone beneath the char layer were neglected.

Structural Integrity

The apparent structural integrity of the models during exposure was indirectly determined from visual observations of the motion pictures, and by examination of the substrate material following exposure. Specimens were sectioned in a plane normal to the surface, and examined visually under magnification for cracks or delaminations which may have propagated internally during or after the exposure period. The presence of char material near the profile of an internal crack was used as a criterion for determining whether cracks were formed during or after the exposure period.

Thermal Insulation

Penetration of heat into the substrate material during ablation was used as a criterion for determining the relative thermal insulation characteristics of the test materials.

Specimens were sectioned in a plane normal to the surface, and the cross-section examined under magnification for evidences of thermal degradation. The nature and extent of damage in the substrate was determined from visual observations and various physical measurements. Attention was focused on the surface char layer and the volatile loss region immediately beneath the char layer. This latter zone of damage was exposed for observation by evaporating acetone from the polished surface.

Cross-sectional views of the ablated models were photographically recorded. In addition, enlarged detailed photographs were taken of the cross-sections of the thermal damage zones. Char surface material, which separated from the models after exposure, was butted to the models prior to photographing.

Pyrolyzed Surface Material

Chemical composition and physical nature of the degraded surface materials were determined by X-ray diffraction analysis. The apparent structure and porosity of the char material were also noted from surface and cross-sectional photomicrographs enlarged 16.0 and 10.6 optical diameters, respectively.

The amount of carbonaceous material on each specimen was measured gravimetrically after removal from the model. Sections of the degraded material were then taken at the apex, middle and aft locations on the exposed models, and density measurements performed in the following manner. The weight of the small porous sample was determined using an analytical

balance. The sample was then immersed in a reference volume of 20-mesh tin granules, and the displaced tin granules weighed. From a knowledge of the apparent density of the tin granules, the volume of displaced tin was computed. This was equal to the volume of the carbon sample. Having determined the mass and the volume of the carbon sample, the density was then calculated.

The volume of voids in the porous char layer was a matter of practical importance since gases of pyrolysis pass through this degraded layer during ablation. This value was calculated in terms of percent porosity of the char layer using the following relation:

$$\% \text{ porosity} = 1 - \frac{\rho_c}{\rho_{imp}} \times 100 \quad . \qquad (2)$$

Where:

ρ_c = density of char layer
ρ_{imp} = density of impervious carbon.

A value of 2.02 gm/cc was used as the density of impervious carbon.

SECTION VII

EXPERIMENTAL RESULTS

Model Performance during Ablation

Y-31 Phenolic-Nylon Resin was flash pyrolyzed from the surface of the model immediately upon exposure to the plasma stream. The ablating surface then became a network of voids closely resembling the original weave of the nylon fabric reinforcement. Continued exposure obscured this surface pattern and a smoother appearance was noted.

Small pieces of material were spalled from the model during the first ten seconds of exposure. The resultant surface voids rapidly disappeared with additional exposure time, and were not apparent at the end of test. No liquid formation was observed during test.

The exposed model surface emitted a brilliant glow after several seconds exposure, and continued this incandescence throughout the remainder of the test period. This effect was attributed to radiant emission in the visible spectrum from the hot ablating surface.

Structural integrity of the specimen was maintained throughout air plasma exposure, and no cracks or delaminations were observed. Dimensional changes were minor, with most of the ablation occurring in the apex region. Asymmetrical ablation of the model was encountered because of the variation in orientation of the reinforcement with respect to the gas stream.

Y-32 Phenolic-Nylon Photographic coverage of this specimen was obscured by inadvertent over-exposure of the motion picture film. Nevertheless, certain data were obtained.

General appearance of the Y-32 model during ablation closely resembled that of the preceding specimen. This type of behavior was anticipated in view of the similar chemical composition. Unlike the preceding specimen, however, no spalling was obtained during exposure of the Y-32 specimen.

Y-33 Melamine-Nylon Flash pyrolysis of resin from the model surface took place immediately upon exposure to the plasma stream. The surface acquired a pebble-grain appearance, with subsequent formation of small clumps of pyrolyzed material. These clumps disappeared with continued exposure, and the surface of the model developed irregularities.

During specimen exposure, no structural failures or surface spalling were detected. Geometric configuration appeared to remain uniform, with some distortion in the apex region.

Boundary Layer Shielding

With the aid of high speed color photography, qualitative observations were made of the region surrounding the models during ablation. Gases formed in the thermal decomposition of material were ejected into the boundary layer, and a significant increase in the thickness of this layer was noted. The boundary layer appeared to be thinnest at the specimen apex, and increased in thickness with distance from the stagnation point. All of the ablating models appeared to have about the same boundary layer thickness, even though the weight of gaseous products formed by the various models was significantly different.

Thickening of the boundary layer with gaseous products alters the convective heat transfer to the model. The resultant effect is commonly known as "boundary layer shielding."

Post-Exposure Appearance

External views of the specimens after 30 seconds exposure are shown in Figures 4 and 5. Each specimen contained a black, porous carbonaceous surface material. The char was a network of voids, which closely resembled the original weave of the nylon reinforcement.

All specimens exhibited relatively good retention of geometric configuration, except in the stagnation region. Apexes of the models became successively more blunt during exposure and their radii of curvature changed from an initial 17/32-inch to about 27/32-inch. Slight necking of the Y-31 and Y-33 specimens occurred in the region where the spherical tip meets the 45° angle portion of the model.

The char layer on the exposed models separated from the solid substrate during post-exposure handling. Apparently, the mechanical bond between the char layer and the substrate was very weak. A reasonable

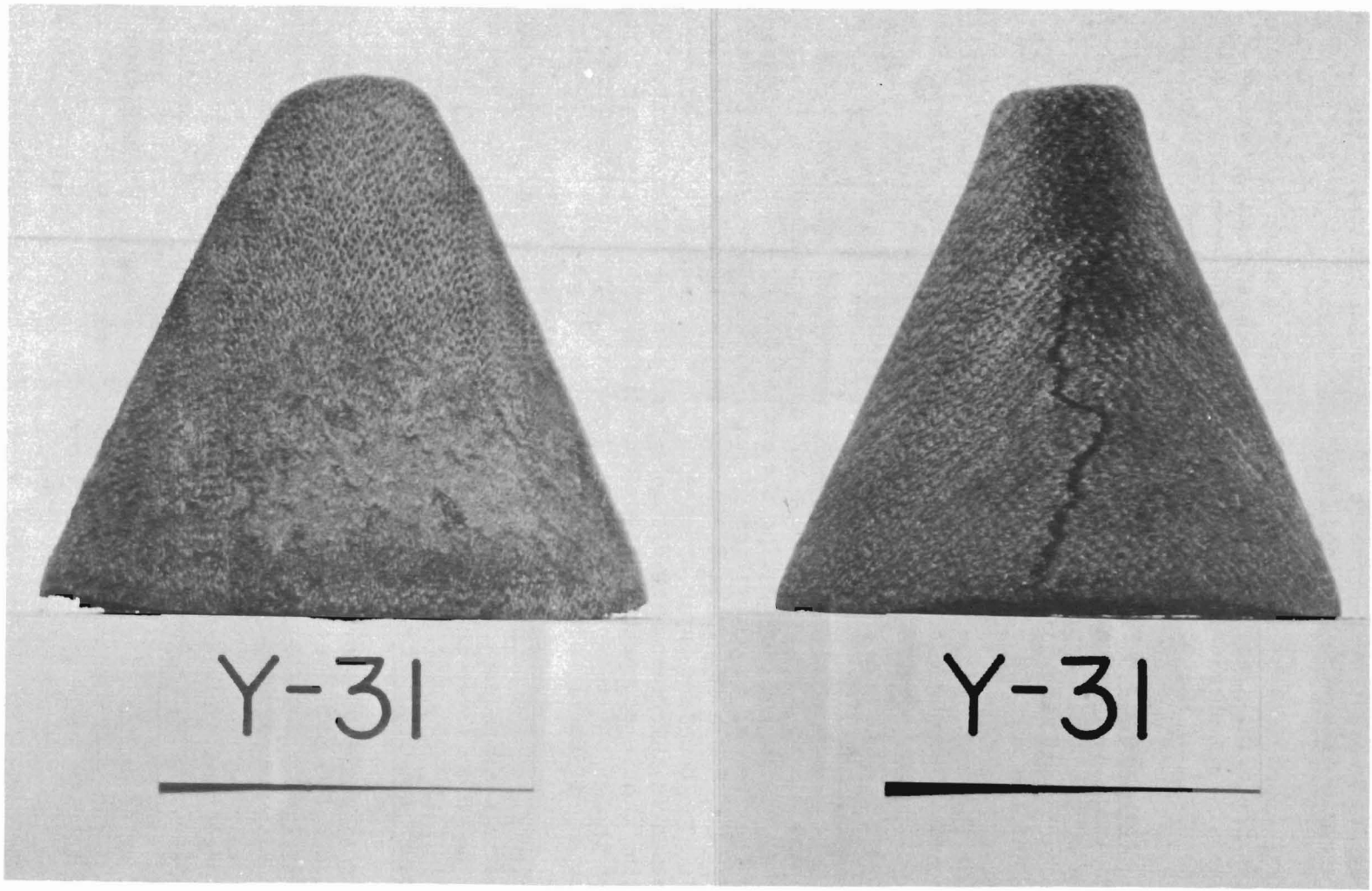

Figure 4. External Appearance of the Ablated Y-31 Specimen (Photograph on the Right is 90° from That on the Left)

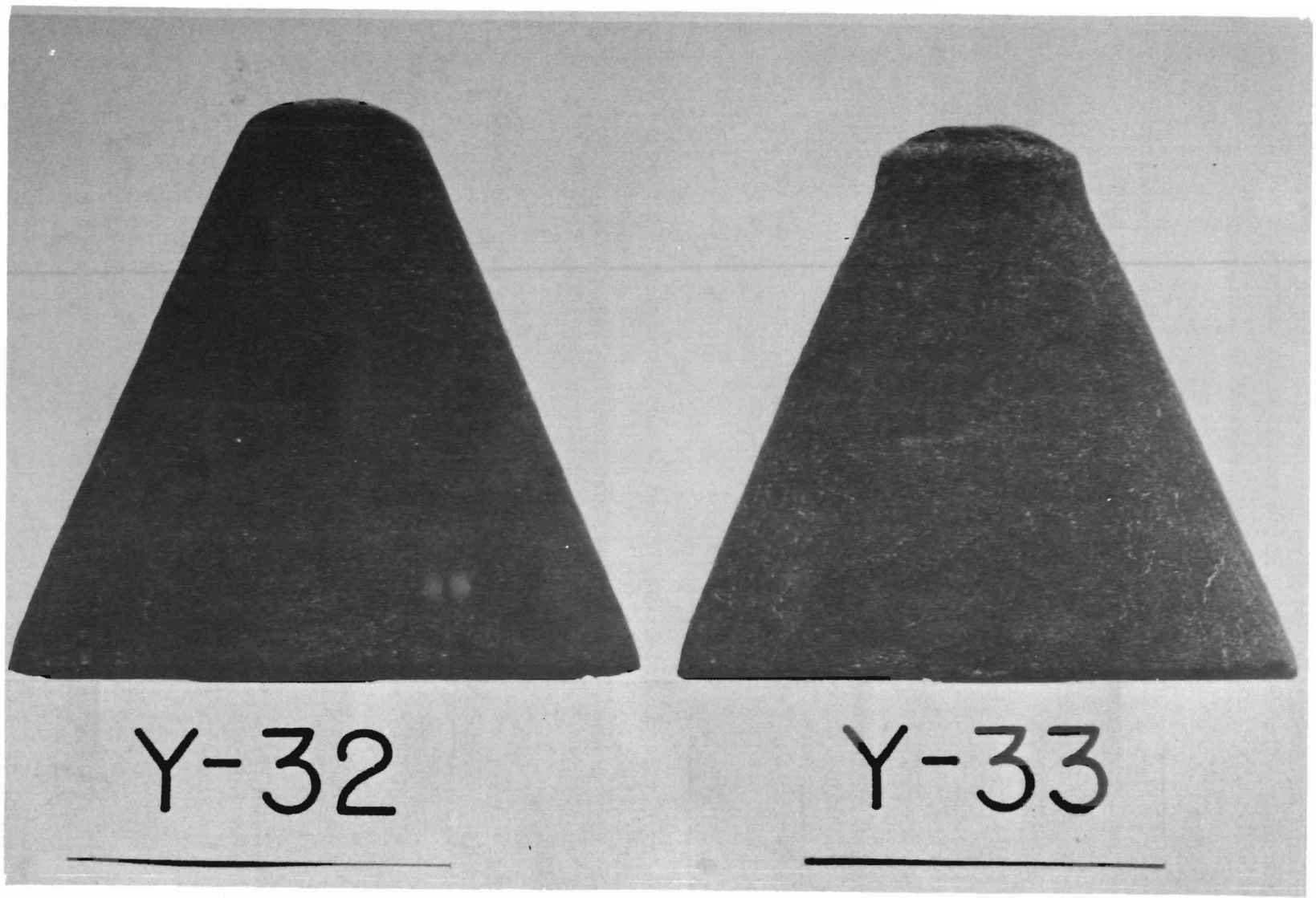

Figure 5. External Appearance of the Y-32 and Y-33 Test Models after 30 Seconds Exposure to the Air Plasma

explanation for this condition involves shrinkage of the hot carbonized surface immediately after exposure, which resulted in large thermal stresses at the interface.

Profile Changes

Figures 6, 7, and 8 are two-dimensional profiles of the specimens taken before and after exposure.* The extent of ablation, as shown in gray on the photographs, appeared to be most evident in the Y-31 test model. Ablation of the Y-33 and Y-32 specimens was less pronounced, in that order of decreasing magnitude.

Further inspection of the profile photographs will show significant ablation and geometric changes in the stagnation point region. Uniform ablation was obtained over most of this region on the Y-32 specimen, but the apexes of the Y-31 and Y-33 models were asymmetrically ablated.

Orientation of the reinforcement in the Y-31 specimen, which was parallel to the major axis of the cone, did not appear to significantly affect the ablation rate. This type of performance is in contrast to resin oriented-vitreous fiber constructions where minimum attrition is obtained when the plane of reinforcement is normal to the hot gas stream.

Thermally Degraded Surface

A black pyrolytic material was formed on the exposed surface areas of the models during test. Examination under magnification revealed that its structure was very porous, filamentous, and interlocking. This can be readily seen in Figures 9, 10, and 11, which are photomicrographs of the model surfaces.

The total amount of carbonaceous material on the exposed specimens was determined gravimetrically, and results were as follows:

Specimen	Char Layer Weight
Y-31	17.3 gm
Y-32	21.5 gm
Y-33	5.5 gm

The amount of residual carbon on the exposed surfaces is presumably affected by many factors.

Specimen	Weight Percent Carbon
Y-31	64.8
Y-32	69.3
Y-33	51.2

* Misalignment of the double exposure photograph was inadvertently obtained.

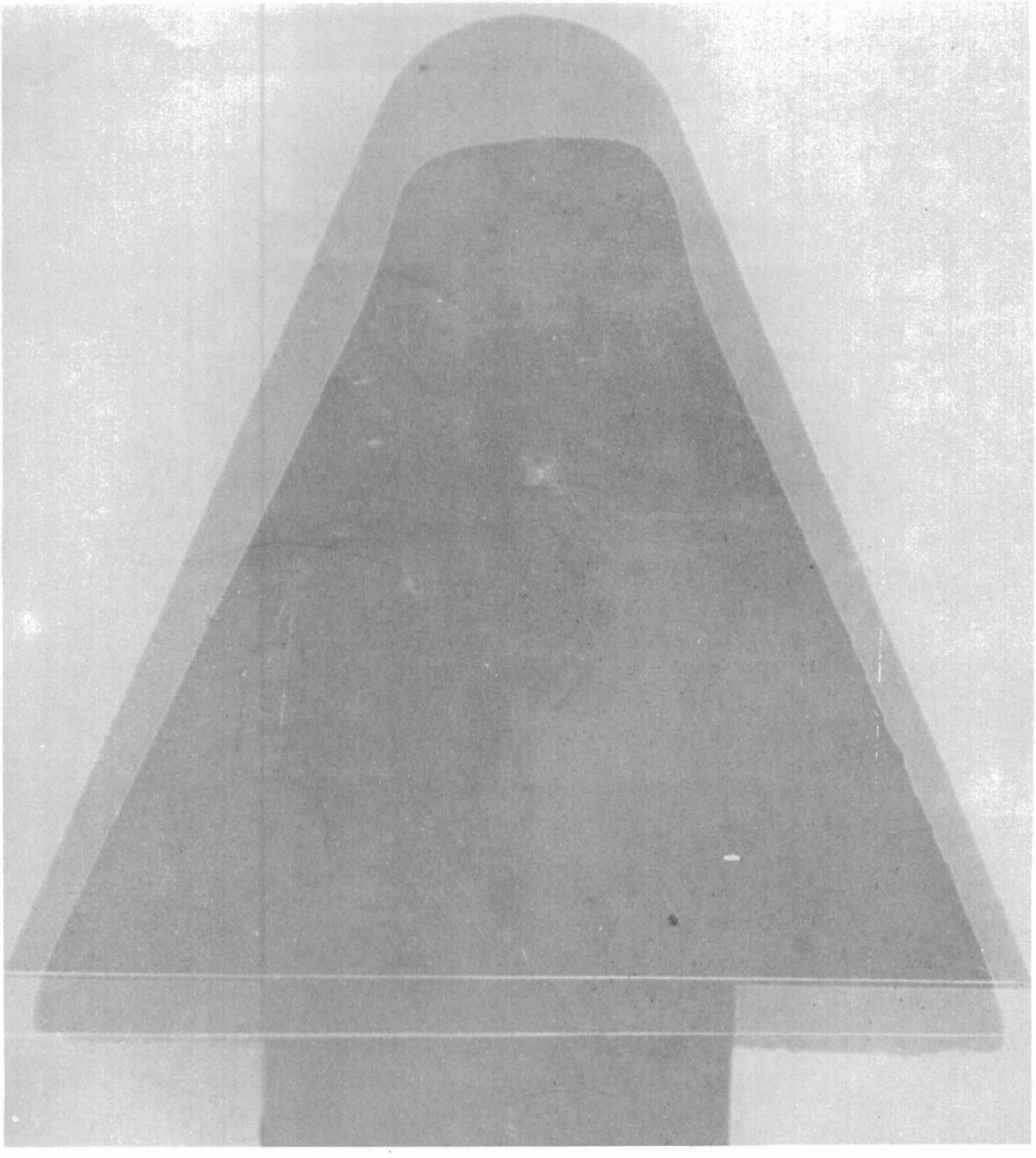

Figure 6. Profile of Y-31 Specimen before and after Air Plasma Exposure (Eroded Area Is Shown in Gray)

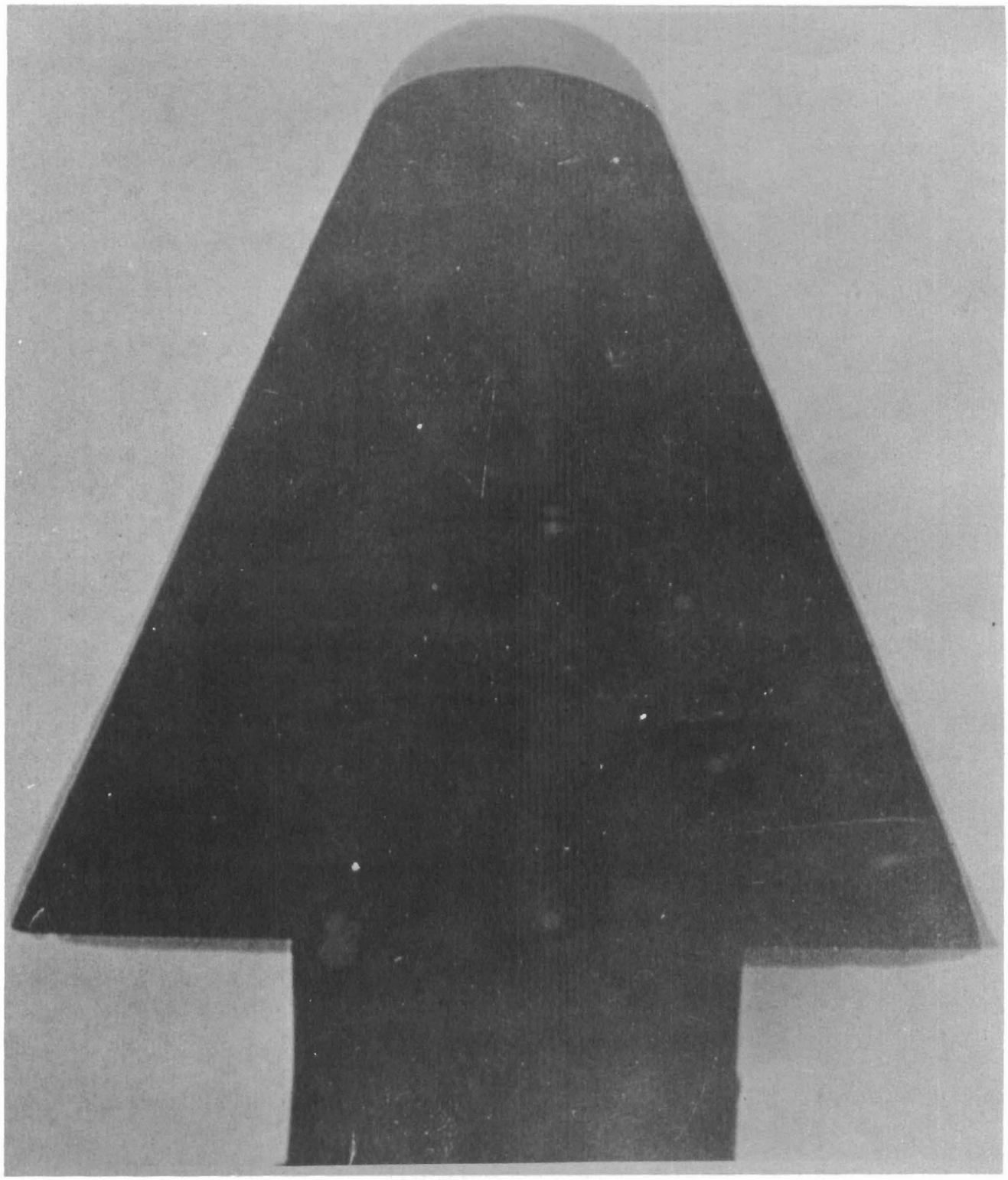

Figure 7. Profile of Y-32 Specimen before and after Air Plasma Exposure (Eroded Area Is Shown in Gray)

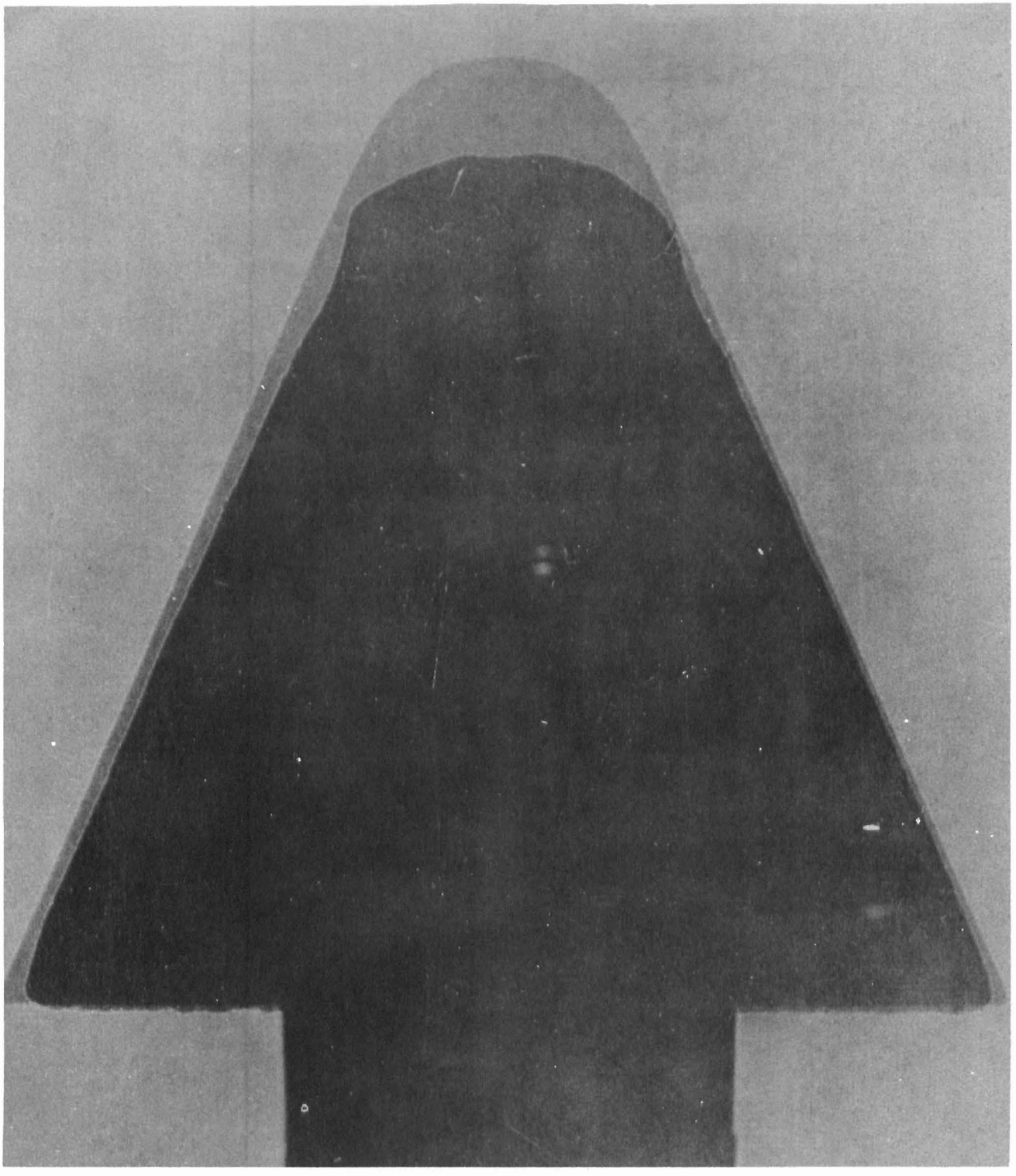

Figure 8. Profile of Y-33 Specimen before and after Air Plasma Exposure (Eroded Area Is Shown in Gray)

Figure 9. Carbonaceous Surface of Y-31 Specimen after Air Plasma Exposure (Enlarged 16 Optical Diameters)

Figure 10. Carbonaceous Surface of Y-32 Specimen after Air Plasma Exposure (Enlarged 16 Optical Diameters)

Figure 11. Carbonaceous Surface of Y-33 Specimen after Air Plasma Exposure (Enlarged 16 Optical Diameters)

Consideration of the weight percent of carbon in the original material will show that the specimen with the highest initial carbon content (Y-32) also contained the most char material after exposure. Other important factors which may affect the amount of residual carbon include the percentage of carbon ablated as hydrocarbon fragments, strength of the surface char, and oxidative resistance of the carbonized material.

A remarkable similarity in physical structure of the degraded surfaces was noted for the Y-31 and Y-32 specimens. In contrast to these two specimens, disconnected clumps of pyrolyzed material were formed on the exposed surfaces of the Y-33 specimen. These clumps were identified as thermally degraded nylon fabric, which was formed after pyrolysis and near complete volatilization of the melamine resin.

The degraded surface material on the exposed specimens was analyzed for chemical composition and physical form. It was determined that the material was carbonaceous in composition and predominately amorphous in physical structure. A slight degree of crystallinity was detected, but this may be attributed to incomplete degradation of the nylon fabric.

Density measurements were made of the char layer to provide an indication of porosity and strength. Sections of the carbonized layer taken from the aft, middle and apex positions on the specimens had density values shown in Figure 12. The density of the char layer did not vary significantly with position on the specimen, but considerable differences were noted between materials. Average apparent densities of the char layer for the Y-31, Y-32 and Y-33 models were 0.44 gm/cc, 0.39 gm/cc and 0.19 gm/cc, respectively.

Only qualitative strength measurements were obtained on the carbonized surface materials. Observations of handling, crushing, and compressive characteristics indicated that the strength varied in accordance with the density. Char material having the highest density appeared to have the highest strength.

The percent porosity, or total volume percent of voids in the char layer was determined with the aid of equation (2). Results were:

Specimen	Percent Porosity
Y-31	78
Y-32	81
Y-33	91

Thermal Damage Zones

Cross-sections of the specimens were examined to determine the extent of thermal damage by air plasma exposure. Three distinct damage zones were identified. First, surface material was physically removed from the specimen by thermal-chemical-mechanical erosion. Second, pyrolysis of the surface plastic produced a porous degraded layer which was retained on the model. Third, volatile losses from the substrate immediately below the char layer produced a third zone of damage.

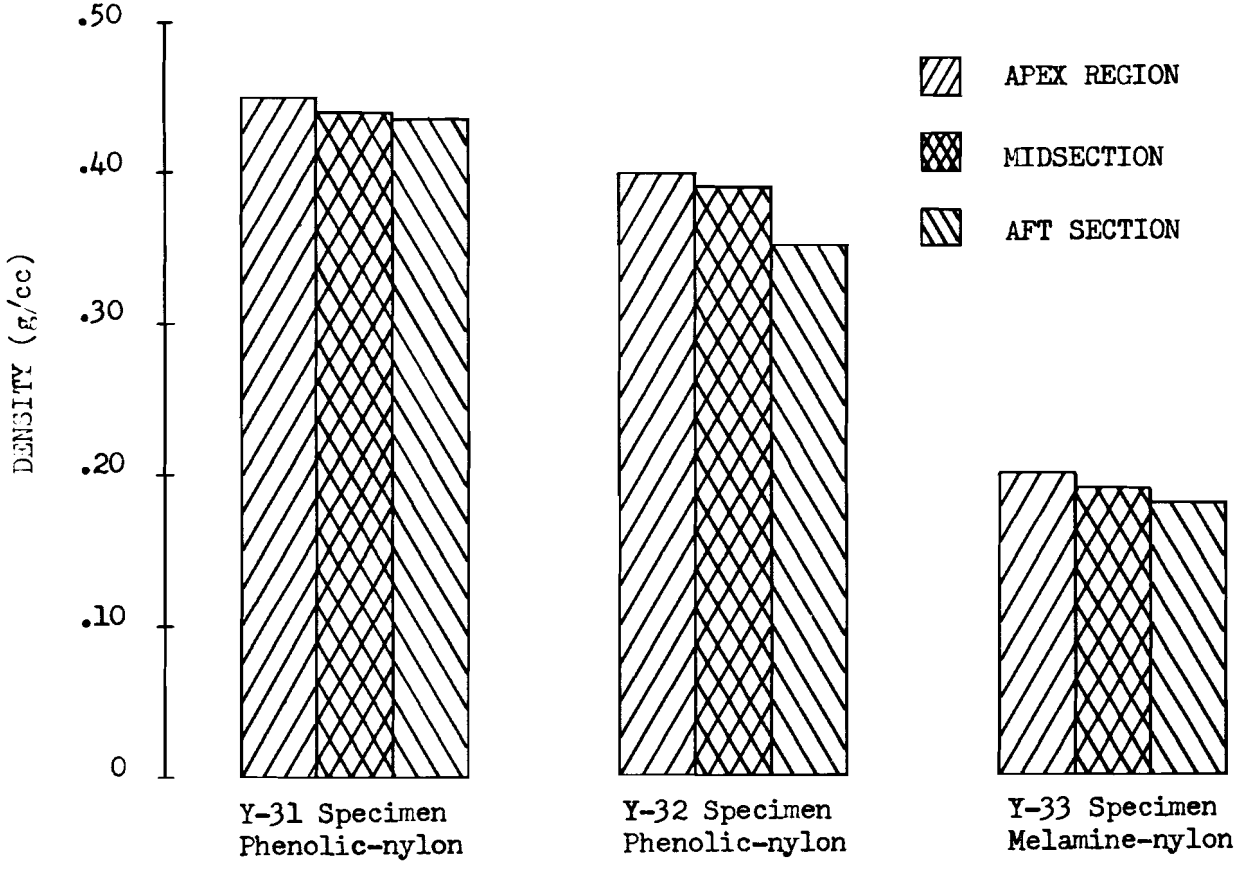

Figure 12. Densities of the Char Layer at Various Positions on the Exposed Specimens

Figure 13 shows the extent of thermal damage at the stagnation point of the models. A summation of the thermal damage zones for each model indicates considerable differences in materials response to the environment.

Actual linear ablation was most severe for the Y-33 specimen and less extensive in the Y-31 and Y-32 models in that order of decreasing magnitude. After 28 seconds exposure, dimensional changes parallel to the model axis were:

Specimen	Linear Ablation
Y-31	0.20 inch
Y-32	0.11 inch
Y-33	0.26 inch

Stagnation point linear ablation of the Y-32 specimen was comparable to several grades of graphite tested under the same exposure conditions. Furthermore, the ablation value was about one-third less than that obtained with typical resin-glass ablative materials.

Porous carbonaceous material on the exposed surfaces extended to various depths into the substrate. Examination of Figures 14 and 15 show a thin char layer near the specimen apex, an increase in char thickness where the model tip meets the 45° angle of the specimen, and decreasing char thickness in the direction of the cone base.

The thickness of the char layer at the stagnation point of the models was measured, and found to be:

Specimen	Char Layer Thickness
Y-31	0.113 inch
Y-32	0.120 inch
Y-33	0.010 inch

Test conditions did not favor the formation of a thick char layer on the Y-33 specimen, in spite of the fact that the original material had a relatively high carbon content. It is believed that the char material formed by thermal decomposition was weakly bonded to the surface. Under such conditions, the char surface material would be susceptible to the mechanical forces of the plasma jet and would be easily removed.

The depth of thermal damage in the zone beneath the char layer was very shallow for all specimens, and varied as follows:

Specimen	Depth of Damage
Y-31	0.05 inch
Y-32	0.02 inch
Y-33	0.01 inch

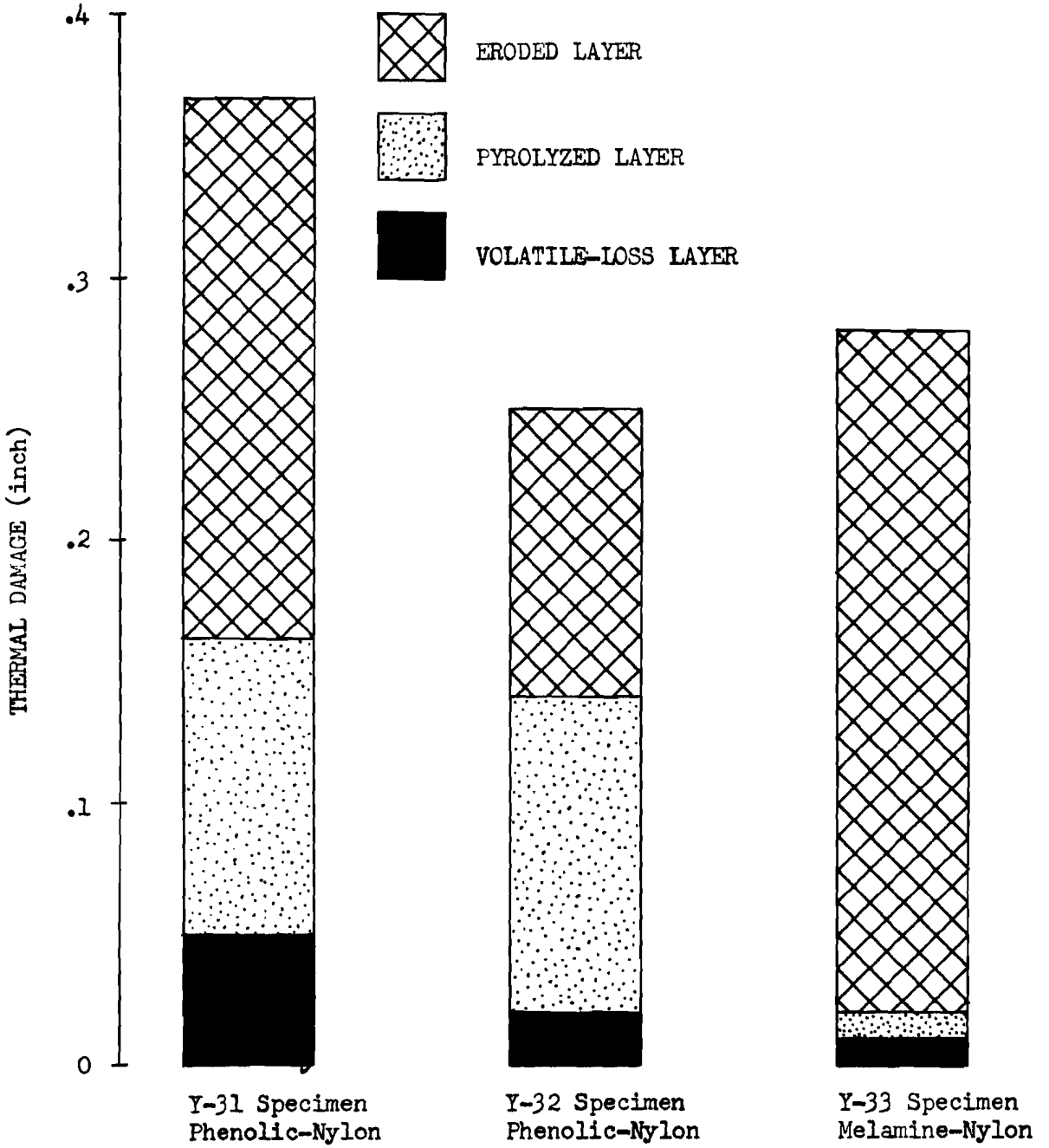

Figure 13. Extent of Thermal Damage to Stagnation Apex Region after 28 Seconds Exposure to Air Plasma

Volatile losses in this zone of damage were due to penetration of heat from the hot char layer into the body, part of which took place after termination of exposure. A slightly greater penetration of heat from the char layer into the substrate plastic was obtained in the Y-31 specimen. This effect was apparently due to the orientation of the reinforcement in a plane parallel to the model axis. The effect was not pronounced, however, since there were only minor differences in the thermal properties of the organic resin and reinforcement components. The low depth of damage on the Y-33 specimen was anticipated in view of the thin char layer retained on its surface throughout test.

Cross-Sectional Examination

Photographic cross-sectional views of the entire specimens are shown in Figures 14 and 15. Examination of the cross-sections of the pyrolyzed and volatile-loss zones were made under low magnification. Typical sections of the various models were photographically recorded, and are shown in Figures 16, 17 and 18.

The surfaces of the exposed Y-31 and Y-32 specimens were relatively smooth, but greater surface roughness was noted on the Y-33 specimen. The char layers on the phenolic-nylon models appeared to be dense and uniformly porous. On the contrary, the char layer on the melamine-nylon specimen was less dense and contained large voids near the interface of the char layer and the solid body. The presence of these large voids indicated rapid volatilization of the melamine resin during test, and subsequent carbonization of the remaining nylon fabric.

Mass Ablation

The rate of mass ablation was determined gravimetrically by averaging total weight loss over the exposure period. Test results were:

Specimen	Mass Ablation Rate
Y-31	2.77 gm/sec
Y-32	2.27 gm/sec
Y-33	2.62 gm/sec

If the mass ablation value is defined as the sum of the material physically removed and the degraded char layer retained on the model, then an adjusted mass ablation value may be computed. Results based on this method of data analysis were:

Specimen	Adjusted Mass Ablation Rate
Y-31	3.38 gm/sec
Y-32	2.98 gm/sec
Y-33	2.81 gm/sec

Hence, the latter mass ablation rate values were between 7 and 31 percent higher than those based strictly on gravimetric measurements.

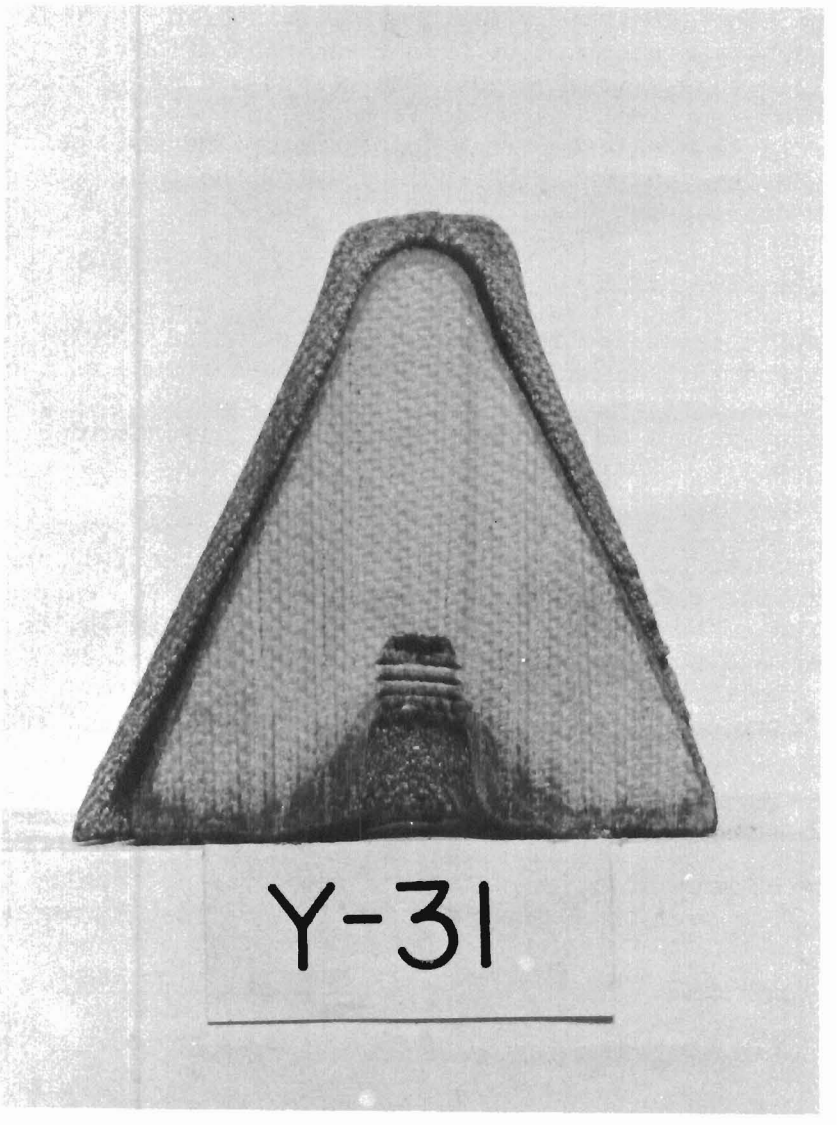

Figure 14. Cross-Sectional View of Y-31 Specimen after Air Plasma Exposure

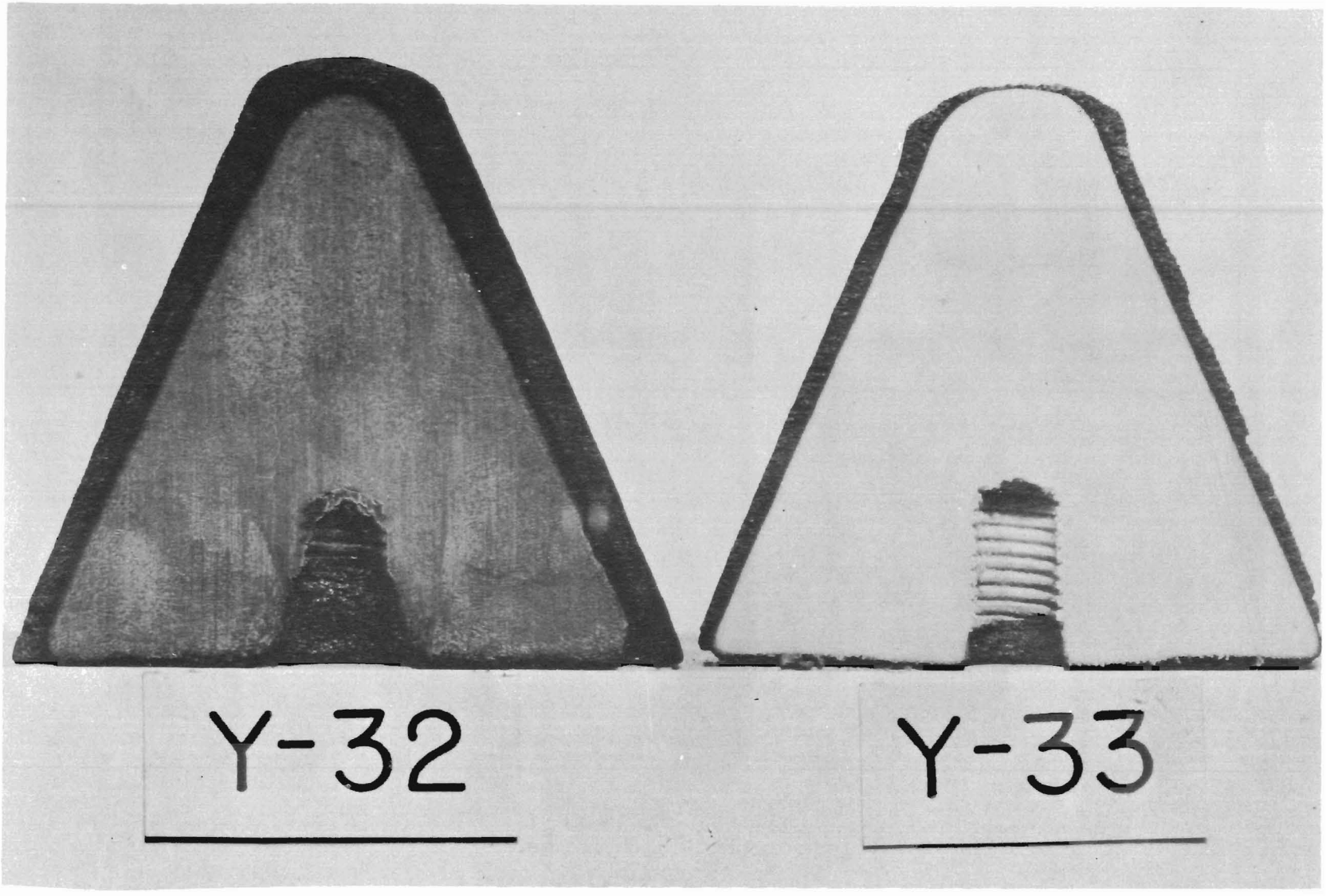

Figure 15. Cross-Sectional View of Y-32 Phenolic-Nylon and Y-33 Melamine-Nylon Specimens after Air Plasma Exposure

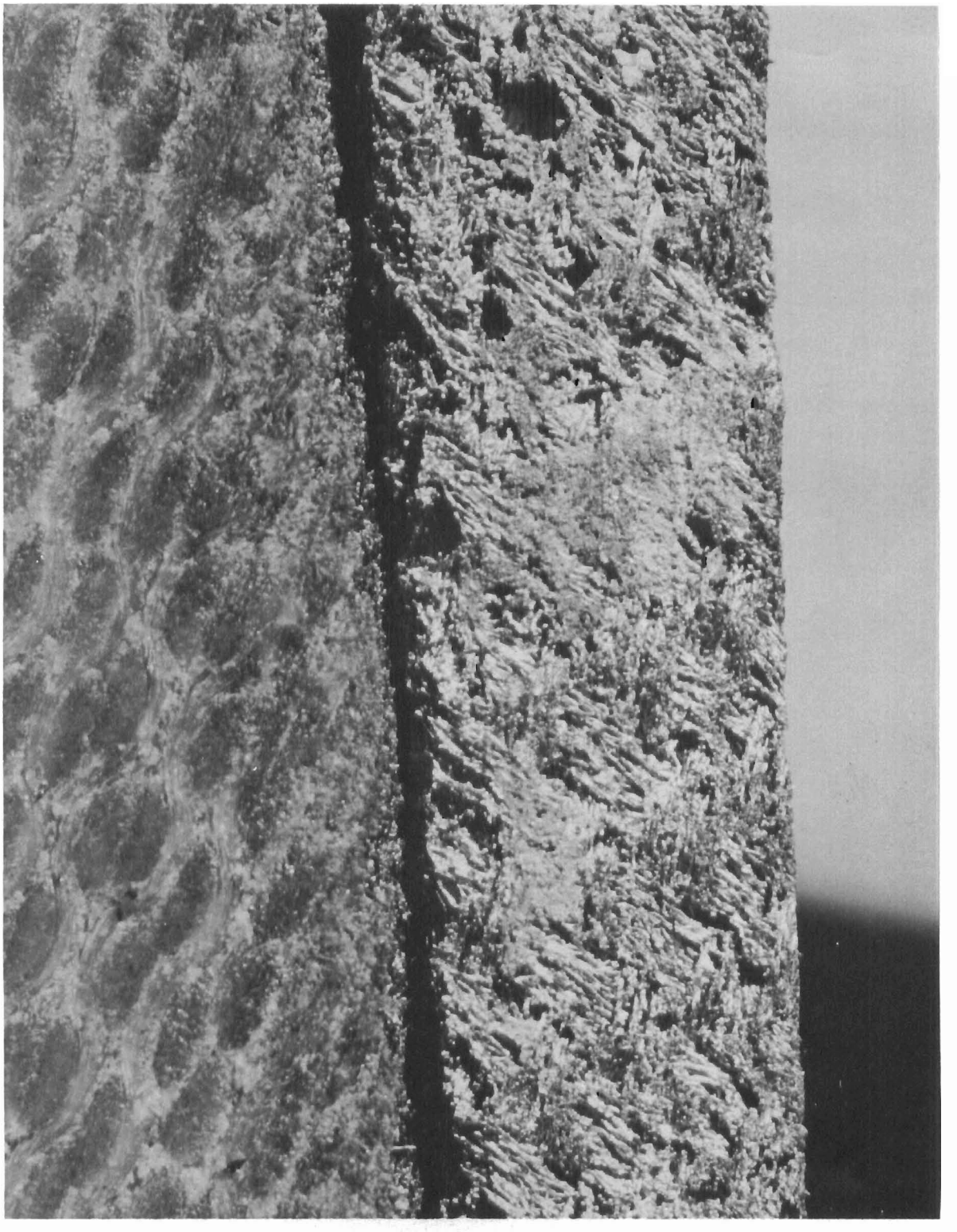

Figure 16. Cross-Sectional View of the Y-31 Specimen after Air Plasma Exposure (Enlarged 10.6 Optical Diameters)

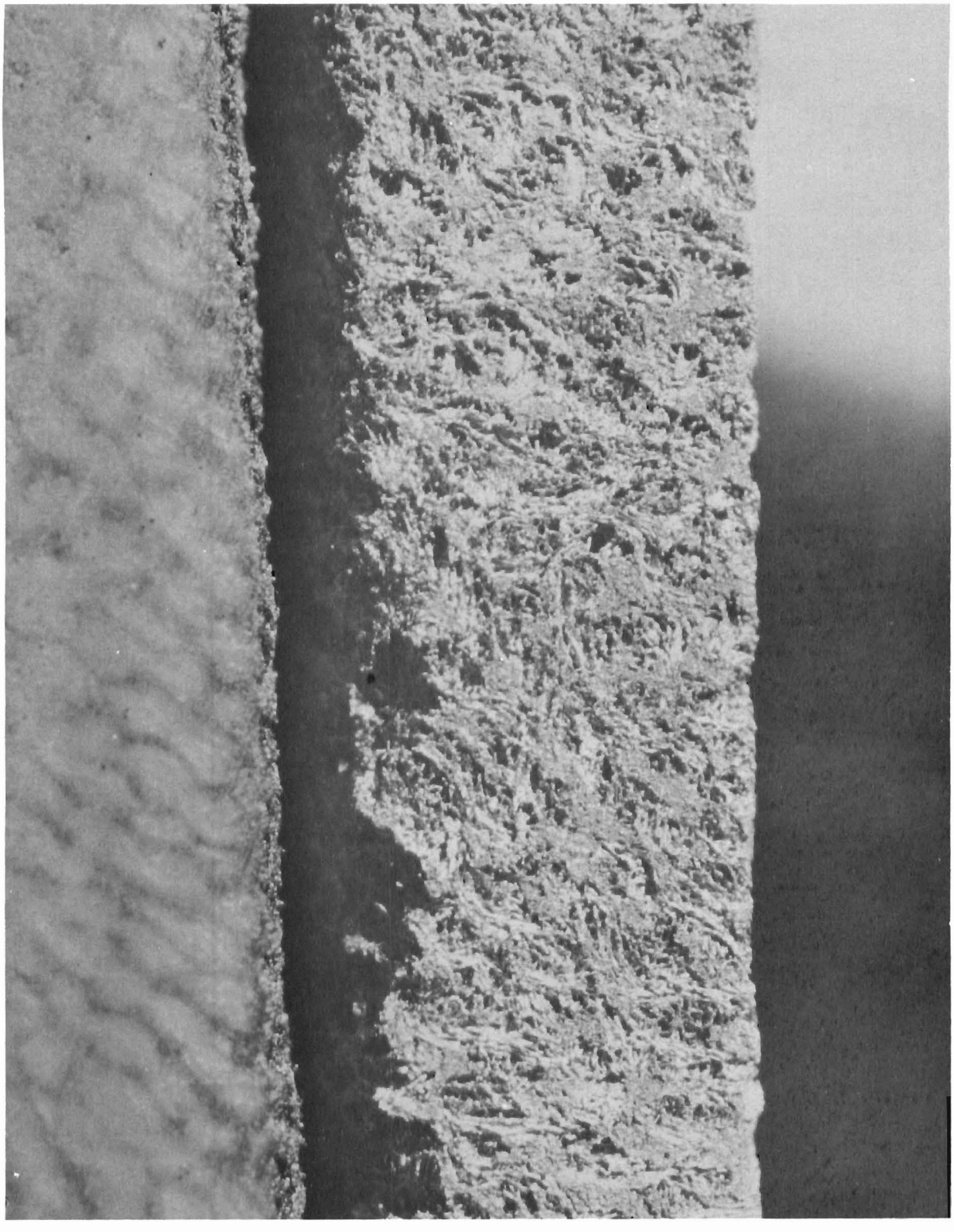

Figure 17. Cross-Sectional View of the Y-32 Specimen after Air Plasma Exposure (Enlarged 10.6 Optical Diameters)

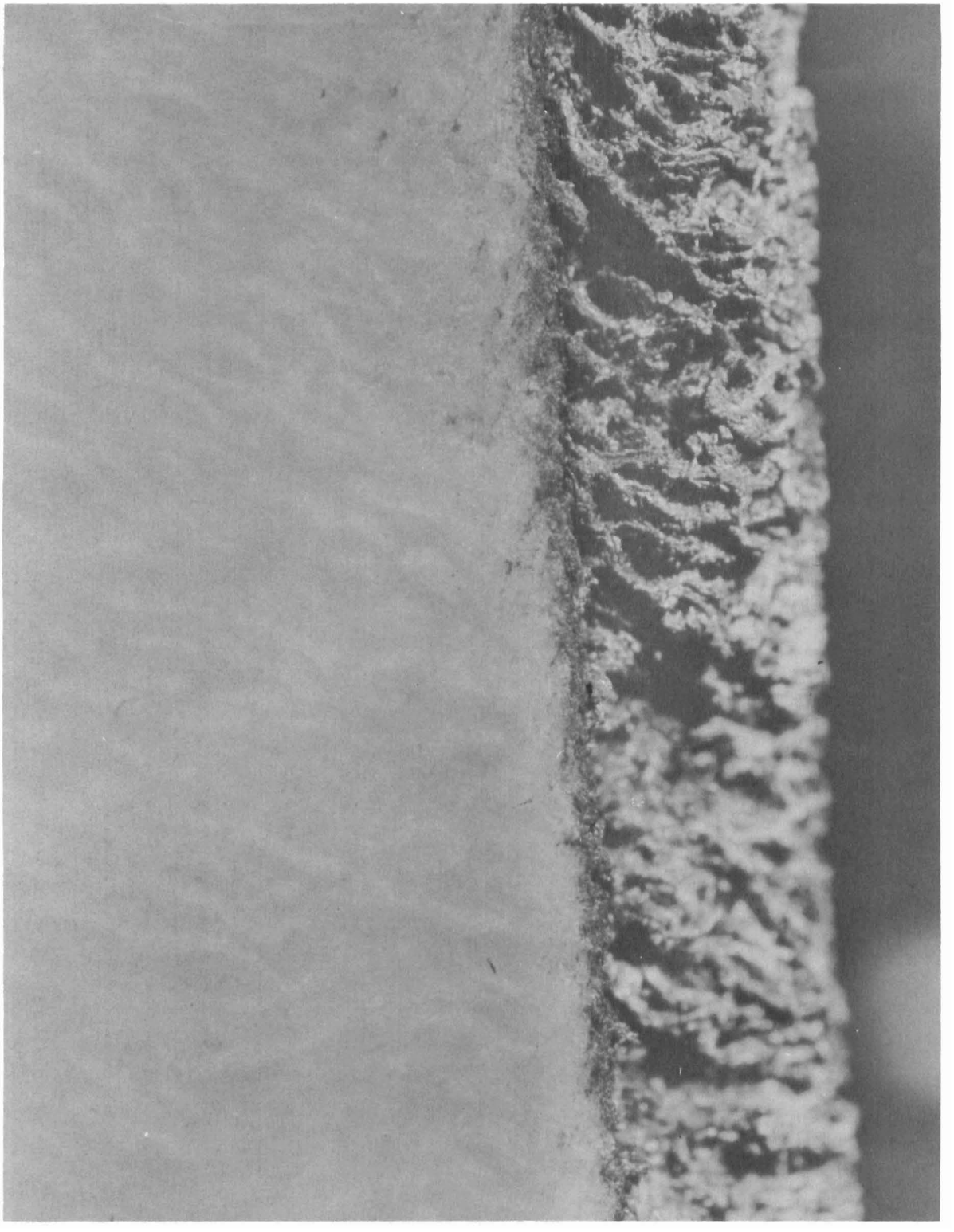

Figure 18. Cross-Sectional View of the Y-33 Specimen after Air Plasma Exposure (Enlarged 10.6 Optical Diameters)

Stagnation point mass ablation rates were also determined using linear erosion measurements taken at the specimen apexes. With the aid of equation (1), the following values were obtained:

Specimen	Stagnation Point Mass Ablation Rate
Y-31	0.0511 lb/ft^2-sec
Y-32	0.0401 lb/ft^2-sec
Y-33	0.0665 lb/ft^2-sec

A comparison of the mass ablation rate values as defined by the preceding three methods will show that the order of materials performance may change, depending upon the criteria selected and the model position considered.

Stagnation Point Linear Ablation

Figure 19 is plot of linear ablation at the stagnation point of the test models throughout the exposure time. From this plot, it is apparent that stagnation point ablation of the Y-32 and Y-33 models was a near linear function of the exposure time. In other words, quasi steady-state ablative conditions existed and the rate of ablation remained nearly constant throughout the exposure period. On the contrary, the rate of ablation of the Y-31 model increased continuously with exposure time.

The stagnation point ablation of the models over the time interval of 0 to 6 seconds was calculated from Figure 19 and found to be:

Specimen	Initial Linear Ablation Rate
Y-31	0.004 in/sec
Y-32	0.004 in/sec
Y-33	0.010 in/sec

Averaging the linear ablation at the stagnation point of the models over the entire exposure period resulted in the following values:

Specimen	Average Linear Ablation Rate
Y-31	0.0073 in/sec
Y-32	0.0040 in/sec
Y-33	0.0093 in/sec

In view of the geometric changes of the model apexes during ablation, the initial linear ablation rate values may be a better indication of the steady-state linear ablation rate.

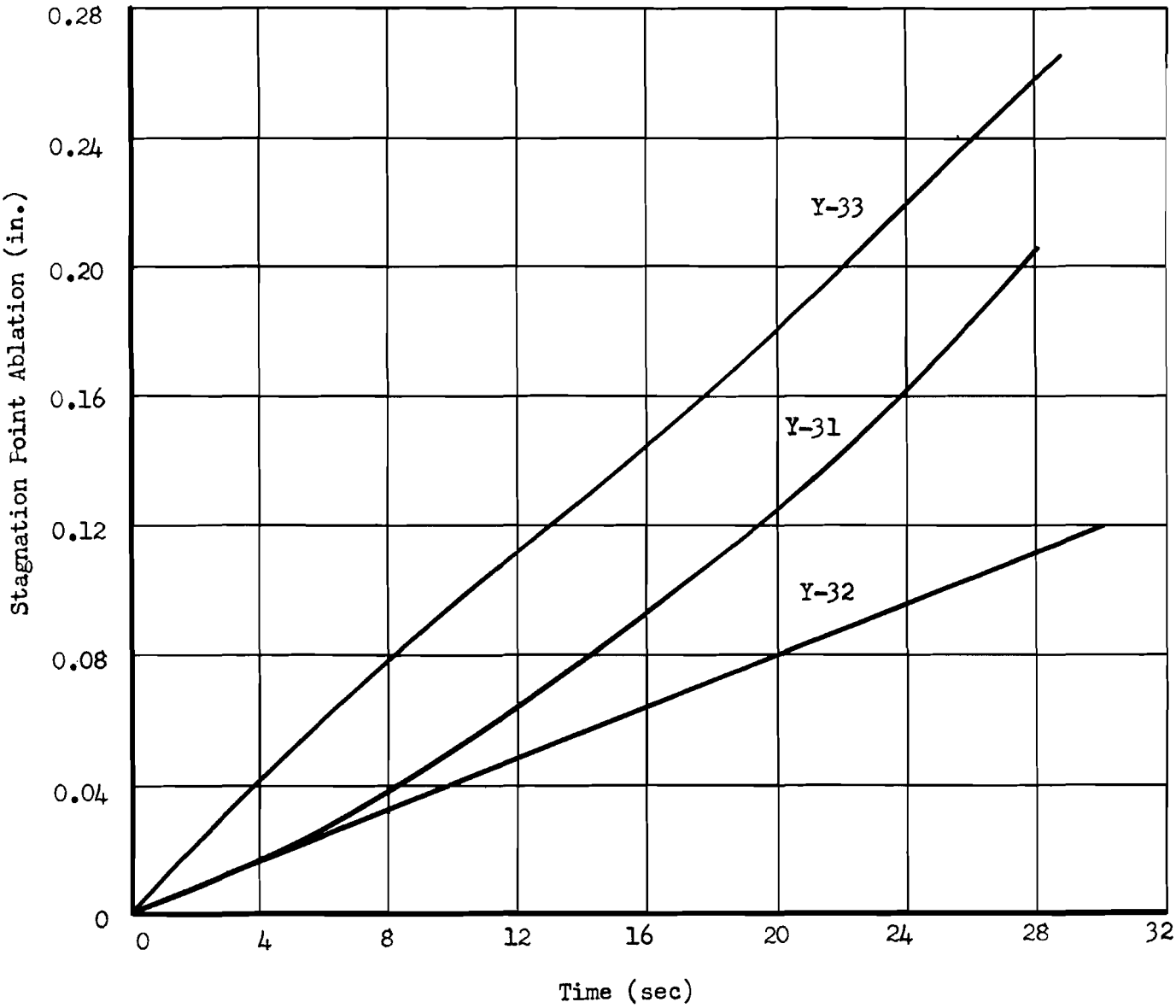

Figure 19. Stagnation Point Linear Ablation During Air Plasma Exposure

SECTION VIII

THERMAL ANALYSIS OF STAGNATION POINT ABLATION

In the preceding section, descriptive information and experimental data were presented on the performance characteristics and physical properties of several organic plastics in an air plasma environment. These results provide important insights into the ablative processes, but offer little information on the mechanisms of thermal protection associated with ablation. The experimental results are re-examined in this section in terms of the heat transfer parameters involved to gain a better understanding of the interaction of the material with its environment. The specific problem to be examined will involve a consideration of the absorptive and dissipative reactions which occur during ablation. Each of the salient exothermic and endothermic parameters of ablation will be discussed, and a numerical estimate of their magnitudes will be given.

Heat Balance for Ablative Plastics

A heat balance equation for ablating plastics was formulated from a consideration of the basic thermal parameters involved. During exposure, heat is transferred to the test models by convection, radiation and conduction. The rate of convective heat input to the test model at the characteristic ablative temperature, but with no mass transfer shall be designated by the term (q_i). Conductive and radiant heat transfer to the model is small and shall be neglected in the analysis. Additional heat is transferred to the test models as a result of chemical reactions in the boundary layer, and both at and within the solid wall material (q_c). Part of the incident thermal flux is dissipated by mass injection of gaseous products into the boundary layer (q_b). Radiant emission from the hot ablating surface also dissipates a portion of the incident flux (q_r). The remainder of the flux input is absorbed by the body (q_a), gaseous products in percolating through the porous degraded surface material (q_g), and by the heats of chemical reactions and physical transformations of the degrading material (q_p). Accordingly, the heat balance equation may be written as:

$$q_i + q_c = q_b + q_r + q_a + q_g + q_p \ .$$

The above parameters will now be treated individually, and a method for estimating their numerical values will be given, where possible.

Hot-Wall Heat Transfer Rate (q_i)

The hot-wall heat transfer rate to the test model was not determined experimentally due to limitations in available calorimeters and instrumentation. It became necessary, then, to compute this value using previously derived heat transfer equations.

Since large temperature gradients existed in the air plasma stream, it was necessary to restrict the heat transfer analysis to the model apex region. Under such conditions, the hot-wall heat transfer rate (q_i) also becomes the stagnation point heat transfer value and will be referred to hereafter as (q_s).

Stagnation Point Heat Transfer (q_s)

The heat transfer analysis of the ablating plastic models was restricted to the stagnation point (apex) region and to steady-state conditions. This particular treatment of the problem is appropriate since steady-state ablation readily lends itself to data analysis. Furthermore, the stagnation point region is of interest since (a) it undergoes intensive convective heating, (b) experimental data were available for this particular region, and (c) considerable information has been published on laminar heat transfer to the stagnation point of blunt bodies in partially dissociated air.

Various aspects of heat transfer to blunt bodies have been previously investigated by Sibulkin (6), Reshotko and Cohen (7), Lees (8), Romig (9), Kemp and Riddell (10), Rose and Stark (11), Fay and Riddell (12) and others. Examination of the heat transfer equations presented by these investigators indicated that the methods of Fay and Riddell (12) and Reshotko and Cohen (7) were best suited for computing the stagnation point heat transfer rate to the test models in air plasma. Both methods are reported to give reasonably good estimates of heat transfer from high temperature air in partial dissociation, and their applicable equations can be numerically solved with ease.

METHOD I

The laminar heat transfer rate at the stagnation point of the hemispherical non-ablating model was determined from a numerical solution of the equation given by Fay and Riddell (12). The equation was derived from stagnation point, boundary layer, nonlinear differential equations using air in dissociation equilibrium, and is given as:

$$q_s = 0.763\, p_r^{-0.6} (\rho\mu)_w^{0.1} (\rho\mu)_s^{0.4} (H_s - H_w) \sqrt{(du/d\bar{x})_s} \left[1 + (L^{0.52} - 1)(H_D/H_s)\right]. \quad (4)$$

Where:

p_r = Prandtl number, partial value
ρ = density of air at the specified conditions
μ = dynamic viscosity of air at the specified conditions
H_s = stagnation enthalpy
H_w = wall enthalpy
$du/d\bar{x}$ = velocity gradient at the stagnation point
L = Lewis number for air-molecule mixture
H_D = average atomic dissociation energy times atom mass fraction.

This simple correlation formula (equation 4) offers a convenient means for computing the stagnation point heat transfer rate from a boundary layer in thermochemical equilibrium. For non-equilibrium conditions of the boundary layer, the heat transfer rate is only slightly affected, provided the Lewis number is near unity and the wall is catalytic (11).

Three important assumptions were necessary in using equation (4) for the test conditions under consideration. First, the thermodynamic and transport properties of the arc-generated air plasma and those of uncontaminated air at the same temperature were taken as being equal to each other. This assumption was necessary due to the near nonexistence of property data on arc-generated plasmas (13). The second supposition provided for thermochemical equilibrium of the plasma at the stagnation point of the model. This condition is reasonable in view of the relatively high (atmospheric) pressure of the test plasma. The third assumption involved a constant Lewis number through the boundary layer at a value of unity.

The accuracy of the heat transfer equation, then, is dependent upon the above assumptions and the accuracy of the thermodynamic and transport properties used in its solution. Precise thermodynamic property data on high temperature air are readily available in the literature, but available knowledge of the transport properties of air is very limited. In the light of the uncertainties discussed, it is clear that the calculated stagnation point heat transfer rate will be only an engineering approximation of the true value.

The stagnation point heat transfer equation may now be expressed as:

$$q_s = 0.94 (p\,\mu)_w^{0.1} (p\,\mu)_s^{0.4} (H_s - H_w) (du/d\bar{x})_s^{0.5} \qquad (5)$$

for an equilibrium boundary layer involving variable fluid properties, a Lewis number of one, and a Prandtl number of 0.71. The individual terms of equation (5) were evaluated (see also Appendix III) at the following experimental conditions:

t_w	=	wall temperature	= 5,000°F
t_o	=	free-stream temperature	= 14,940°F
t_b	=	solid body temperature	= 75°F
u_o	=	free-stream velocity	= 2,500 ft/sec
P_o	=	ambient pressure	= 14.7 psi
D	=	model apex diameter	= 0.0833 ft

using the data given in reference (14). The appropriate values were then substituted into equation (5), and a stagnation point heat transfer rate of 716 Btu/ft^2-sec was obtained.

METHOD II

Heat transfer to the forward stagnation point of the non-ablating model was also determined using the Reshotko and Cohen relation given in reference (7). This relation is based on the conventional heat transfer equation:

$$q = h\,(t_o - t_w) \quad . \tag{6}$$

Where:

h = coefficient of heat transfer
t_o = free-stream or recovery temperature
t_w = temperature at the wall.

For the stagnation point of the experimental models, the heat transfer coefficient becomes:

$$h = (Nu/\sqrt{Re_w})\ (C)_s^{0.5}\ k_w/(\upsilon_w)^{0.5} \quad . \tag{7}$$

Where:

k_w = thermal conductivity of air at t_w
υ_w = kinematic viscosity of air at t_w
$Nu/\sqrt{Re_w}$ = dimensionless heat transfer parameter
C_s = approximation of the velocity gradient at the stagnation point.

By combining equation (6) and (7), the heat transfer equation becomes:

$$q_s = (Nu/\sqrt{Re_w})\ (C)_s^{0.5}\ k_w\ (t_o - t_w)/(\upsilon_w)^{0.5} \tag{8}$$

which shall be used in Method II.

In deriving equation (8), the product of the gas density and viscosity through the boundary layer was considered to be constant. For the experimental case, however, the product $(p\mu)$ is believed to vary appreciably through the boundary layer. Thus, some error is introduced in the heat transfer result, the magnitude of which is presently unknown.

Assumptions of boundary layer conditions in Method II were similar to those expressed in Method I. The boundary layer was assumed to be in equilibrium dissociation with variable fluid properties within this region. The Lewis number was assumed to be unity, and the Prandtl number was estimated to be 0.71. Other pertinent suppositions involved a laminar continuum flow and a linear velocity gradient external to the boundary layer.

The method for calculating the stagnation point heat transfer rate is given in detail in Appendix III. By substituting the proper experimental and reference values into equation (8), a stagnation point heat transfer value of 1,000 Btu/ft^2-sec was obtained.

Stagnation point heat transfer rates to the test models during air plasma exposure have now been computed using equations derived by Fay and

Riddell (12) and Reshotko and Cohen (7). Numerical results of 716 and 1,000 Btu/ft^2-sec, respectively, were obtained for the experimental conditions being considered. Hence, the heat transfer rate predicted by the two methods varied considerably. A cursory attempt was made to determine which method was more applicable for predicting the heat transfer rate for the test conditions used. It was concluded that this question could not be completely resolved without additional detailed experimental work. A stagnation point heat transfer rate of 1,000 Btu/ft^2-sec was selected as the reference value, because for a Lewis number of one, the selected reference value is believed to be the more accurate since it involved less approximation regarding the real gas properties.

Chemical Reactions (q_c)

During ablation, numerous complex chemical reactions take place in the boundary layer, at the ablating surface, and within the hot substrate of the test models. Within the chemically reactive boundary layer, exothermic recombination of atomic species may take place (15). Foreign species injected in the boundary layer undergo gas phase reactions, with liberation of thermal energy to the surroundings (16). Oxygen present in the boundary layer diffuses to the carbonaceous ablating surface and reacts exothermically to form carbon monoxide and carbon dioxide. If the ablating wall is catalytic, atom recombination may occur with the heat of recombination being transferred to the wall particle (17). Finally, heat may also be transferred to the ablating model by subsurface oxidation reactions of the gaseous hydrocarbon fragments.

An exact numerical solution of the chemical heat contributed by each of the above reactions is intractable, due to our lack of knowledge of boundary layer chemistry and the interaction of hyperthermal environments with products of ablation. Past investigations have shown that atomic recombination in the boundary layer and at the wall may contribute significantly to the total incident heat transfer. The process is not well understood and no estimate of the exotherm can be given. The combustion of gases in the boundary layer and at the material boundary has also been examined cursorily, and found to contribute little to the heat content of the environment (18). The effect of combustion was insignificant because of the large stagnation enthalpy already present in the boundary layer. Reactions of the gaseous hydrocarbon fragments with oxygen in the char substrate and oxidation of the carbonaceous surface material may also liberate heat to the system. For the latter reaction, the net exotherm was estimated to be in the order of 75 Btu/ft^2-sec (5).

Boundary Layer Shielding (q_b)

Mass injection of gaseous products into the boundary layer reduces the convective heat transfer to the ablating model. The amount of thermal energy dissipated by this protective mechanism has been examined by several investigators, and their results are given in reference (7, 19, and 20). From these studies, the following empirical relation can be derived:

$$q_b = \dot{m} \left[0.667 \, (M_a/M_g)^{0.26} \, (H_s - H_w) \right] . \qquad (9)$$

Where:

$\dot{m}$ = mass rate of ablation
M_a = molecular weight of undissociated air
M_g = molecular weight of injected gaseous products
H_s = stagnation enthalpy
H_w = wall enthalpy.

Essentially the same result as given in equation (9) has been previously reported in references (18, 21).

A numerical solution of equation (9) requires a knowledge of the average molecular weight of gaseous products injected into the boundary layer. For cases involving ablation, decomposition products in various oxidized states effuse into the boundary layer from the degrading substrate plastic. These gaseous species diffuse outward through the boundary layer, and undergo numerous chemical transformations due to the presence of high temperatures and available thermal energy. Consequently, the chemical identity and molecular weight of the individual gaseous components at the wall and in the boundary layer are a matter of conjecture. Nevertheless, reasonably good approximations of the molecular weight values may be obtained experimentally by sampling or surveying the boundary layer region with a mass or emission spectrometer. In the absence of suitable analytical equipment, the average molecular weight of the gaseous products may be estimated from a consideration of the origin of the gases and the thermochemical conditions existing at the wall. This latter approach was taken in the treatment of the problem.

The average molecular weight of the injected gaseous products was determined in the following manner. The elemental composition of the solid organic material was determined using micro-combustion analysis. These data along with a consideration of possible chemical reactions and product interactions occurring during ablation indicated the probable gaseous products. Literature on the thermal degradation of polymeric materials was reviewed, and the reaction products established for the test conditions under consideration (22, 23). It was concluded that carbon monoxide, carbon dioxide, water vapor, nitrogen, hydrogen and hydrocarbon fragments were ejected into the boundary layer during ablation. Relative amounts of these gases were determined from the reaction equations established, elemental composition of the solid body, and equilibrium constants for the multicomponent system (24). Volumetric percents or mole fractions of the gases were multiplied by their respective molecular weights, and the sum of the computation yielded the average molecular weight of the injected gaseous products. Results were as follows:

Specimen	M_g
Y-31	36
Y-32	37
Y-33	35

The appropriate values were then substituted into equation (9), and the following values were obtained:

Specimen	Thermal Shielding Value (q_b)
Y-31	265 Btu/ft^2-sec
Y-32	206 Btu/ft^2-sec
Y-33	347 Btu/ft^2-sec

Examination of the experimental results will show that large differences in the boundary layer shielding terms are directly attributable to the respective mass ablation rates of the various specimens. This is necessarily the case for the analysis presented, since the environmental enthalpy potential was equal for all specimens and the average molecular weight of gaseous products varied only slightly between specimens.

The presence of foreign gases in the boundary layer has a secondary minor effect on heat transferred from the hot air plasma to the model surface. The passage of radiant energy through the pyrolytic gases formed by ablation may be significantly altered, depending upon the composition and concentration of foreign gases present. Carbon dioxide and water are both known to be good absorbers and radiators of radiant energy. Their presence in the boundary layer forms a radiation shield around the model, the importance of which is not presently well understood. Nevertheless, this radiation shielding effect on total heat transfer must be small since the concentration of injected gaseous species in the boundary layer at any time was relatively small.

Radiant Emission (q_r)

Since the surface of the ablating model was at a relatively high temperature, it radiated a significant portion of the incident heat flux. By use of the well known Stefan-Boltzmann fourth power law:

$$q_r = e \sigma t_w^4 \quad . \tag{10}$$

Where:

e = emissivity of the body
σ = Stefan-Boltzmann constant
t_w = temperature of the ablating surface, $^\circ$R

the thermal energy loss per unit time was computed for a wall temperature of 5,000°F (5,460°R).

Emissivity values for porous carbonaceous materials at elevated temperatures are presently unavailable in the literature. Therefore, it was necessary to estimate this value taking into consideration the roughness and porosity of the surface. An emissivity of 0.80 was chosen for the wall conditions.

The radiant emission from the test model at the stagnation point was determined to be 240 Btu/ft^2-sec. Hence, the high ablation surface

temperature permitted by the carbonaceous material was an effective means for dissipating a large portion of the incident flux.

Heat Transfer to the Model with Mass Transfer (q_{ab})

A measure of the actual heat transfer rate to the ablating models may now be determined using the relation:

$$q_{ab} = q_i + q_c - q_b - q_r \quad . \tag{11}$$

Substituting the appropriate values into equation (11), we have:

Specimen	Heat Transfer Rate to Body (q_{ab})
Y-31	570 Btu/ft^2-sec
Y-32	629 Btu/ft^2-sec
Y-33	488 Btu/ft^2-sec

These values, then, represent the amount of heat per unit time that is absorbed in (a) raising the temperature of the solid material, q_a, (b) heats of reaction and phase changes, q_p and (c) sensible heat absorption in raising the temperature of the gaseous products up to the point where they pass into the boundary layer, q_g.

Sensible Heat of Solid Body (q_a)

The internal temperature of the solid model was raised during exposure to the high temperature environment. In the process, heat was absorbed from the environment. The quantity of heat absorbed is known as the sensible heat of the body. It was computed as the sum of heat required to bring the material up to its temperature of pyrolysis and the heat absorbed in raising the temperature of the residual char layer on the model surface.

Reinforced plastics have no one temperature of pyrolysis, but thermally degrade over a fairly wide range of elevated temperatures. Therefore, a single pyrolytic temperature was arbitrarily selected in order to present an amenable numerical solution. The value taken for all materials was 850°F, based on thermogravimetric data reported in reference (25). Thus, the quantity of heat required to bring the solid body up to its temperature of pyrolysis may be computed from the relation:

$$q = \dot{m} \left[(c_p)_b \ (t_{850^\circ} - t_b) \right] \quad . \tag{12}$$

Specific heat values for the experimental materials and over the temperature range of interest were unavailable in the literature. Therefore, an average value of 0.35 Btu/lb-°F was used in the numerical solution of equation (12). Results for the stagnation point were as follows:

Specimen	Sensible Heat Absorption Rate
Y-31	14 Btu/ft^2-sec
Y-32	11 Btu/ft^2-sec
Y-33	18 Btu/ft^2-sec

Additional heat was also absorbed from the environment in raising the temperature of the surface char layer. The rate of heat absorption was a function of the amount of char material formed per unit time, its thermal properties, and its change in temperature. The relationship used for expressing the sensible heat of the char layer during steady-state ablation was:

$$q = \dot{m} (p_c/p_b) (c_p)_c \ (t_w - t_{850^o}) \ . \qquad (13)$$

Values required for numerical solution of the above equation have been previously reported, except for the specific heat of the char layer. An average value of 0.38 Btu/lb-^oF was assumed for the temperature range being considered, based on data reported in the literature for porous, amorphous, carbonaceous material. Substituting the requisite values into equation (13), we have:

Specimen	Sensible Heat of Char Layer Per Unit Time
Y-31	16 Btu/ft^2-sec
Y-32	14 Btu/ft^2-sec
Y-33	25 Btu/ft^2-sec

By combining the numerical results of equations (12) and (13), a sensible heat absorption value for the solid body under steady-state conditions was obtained. Net results for the stagnation point were as follows:

Specimen	Sensible Heat Absorption of Solid Body (q_a)
Y-31	30 Btu/ft^2-sec
Y-32	25 Btu/ft^2-sec
Y-33	43 Btu/ft^2-sec

Hence, it can be readily seen that sensible heat absorption by the solid body was negligible.

Sensible Heat of Gaseous Products (q_g)

During ablation, various gaseous products were formed in the substrate of the plastic models. These gases were forced outwards toward the surface of the model by a pressure gradient existing in the substrate. In passing through the porous char layer, heat was absorbed by the gaseous mixture and its temperature was raised. Associated with this heat exchange process was a lowering of the model surface temperature.

With the present state-of-the-art, the rate of sensible heat absorption can not be precisely determined for gaseous products effusing through the char layer. This condition exists since the temperature and chemical composition of the multicomponent gaseous mixture changes constantly during diffusion toward the ablating model surface. Nevertheless, a consideration of the sensible enthalpy of some of the probable gaseous products will provide some degree of understanding for the problem involved. A plot of sensible enthalpy (heat content change) as a function of temperature was constructed from data given in reference (26) and is shown in Figure 20. These values have been computed for equilibrium conditions using certain ideal gas approximations. The enthalpy values refer to the amount of thermal energy required to raise one pound of gas, with the initial molecular composition shown, from some reference temperature to another selected higher temperature. In applying the data in Figure 20 to ablative material systems, it should be remembered that the sensible heat absorption by the gases of pyrolysis in percolating through the char layer may be only a fraction of the theoretical maximum. This effect is due to nonequilibrium thermal degradation of the organic material, and may also be due to the presence of interfering chemical reactions.

A comparison of the results in Figure 20 will show the tremendous heat absorption capability of hydrogen, on a weight basis. This desirable property of hydrogen along with its low molecular weight is believed to be one of the reasons why organic materials exhibit favorable ablative characteristics.

A first approximation of the sensible heat of the gaseous products was made to determine their relative importance in the total heat transfer process. It was determined that the rate of heat absorption was dependent upon the volatilization loss rate and the increase in enthalpy of the gaseous products in passing through the char layer. A relationship derived for expressing this absorptive flux is:

$$q_g = \dot{m} \left(1 - p_c/p_b\right) \left(c_p\right)_g \left(t_{3000^\circ} - t_{850^\circ}\right) \quad . \qquad (14)$$

Mass ablation and densities values required in the numerical solution of equation (14) have been previously reported. Based on data reported in the literature, an average specific heat value for the gaseous products was assumed to be 0.5 Btu/lb-$^\circ$F. The effective temperature rise of the gases in percolating through the char layer was estimated at 2150°F, using a decomposition temperature of 850°F and a final wall temperature of 3,000°F. Substituting the appropriate values into equation (14), the following results for the stagnation point region were obtained:

Specimen	Rate of Sensible Heat Absorption by Gaseous Products (q_g)
Y-31	31 Btu/ft^2-sec
Y-32	28 Btu/ft^2-sec
Y-33	61 Btu/ft^2-sec

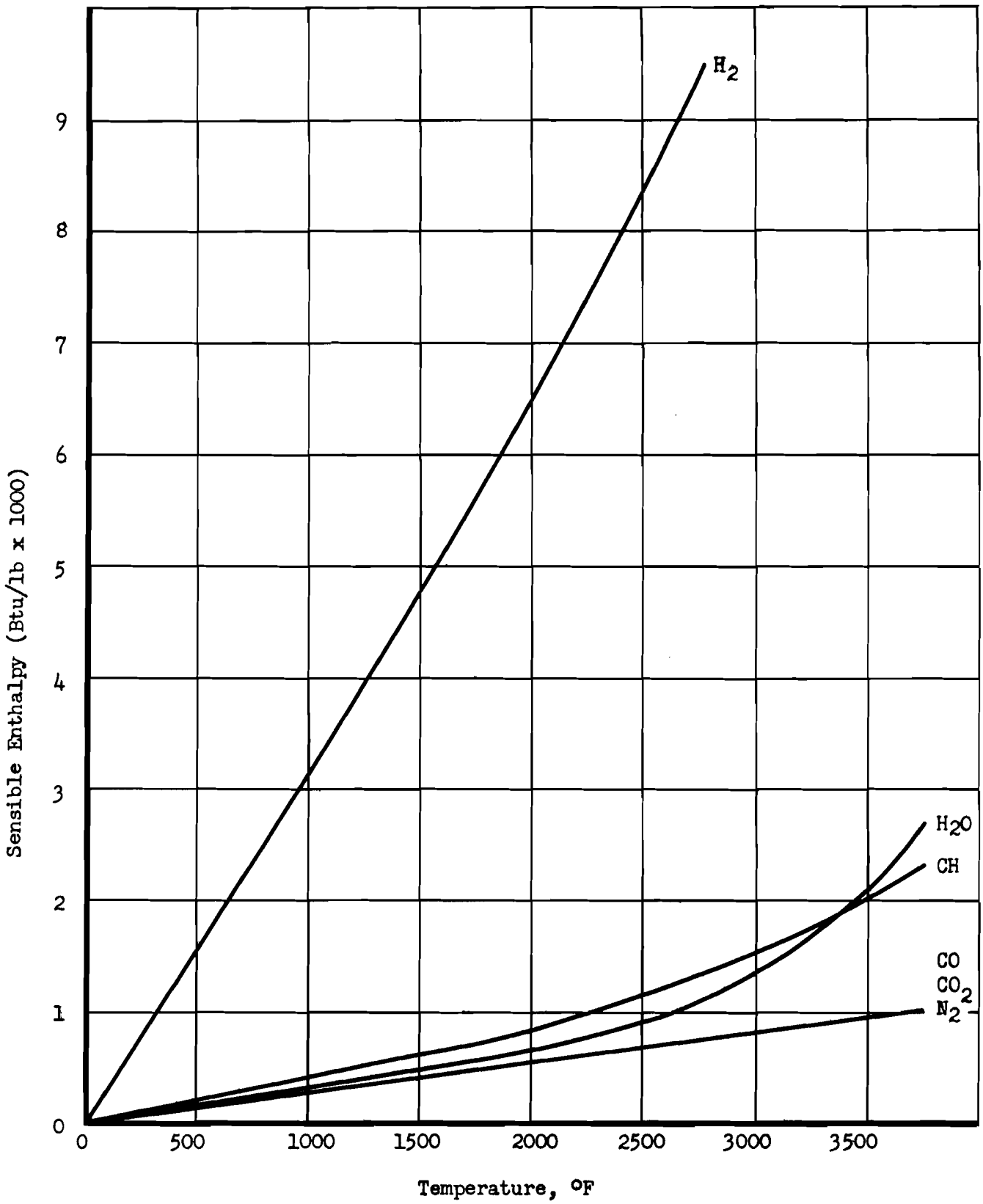

Figure 20. Calculated Sensible Enthalpy for Various Gases at Temperature and Equilibrium Conditions

Hence, the pyrolytic gases of decomposition absorbed only a small fraction of the incident thermal flux as they effused through the surface char layer on the ablating models.

Thermodynamic Chemical and Physical Transformations (q_p)

Numerous complex chemical reactions and physical transformations of the ablative material took place during its interaction with the high temperature air plasma. Depolymerization, pyrolysis, fusion, vaporization and sublimation occurred simultaneously, and at a rate depending upon the incident heat flux, thermal properties of the material, temperature distribution within the body, presence and rate of other reactions occurring in the vicinity, diffusion rate of products from their origin, and similar considerations. The net thermal effect of these chemical reactions and phase changes was to absorb a significant amount of heat from the environment.

Individual latent heats of chemical reactions and physical transformations were not determined experimentally because of the inherent difficulties involved. Instead, the net thermal effect of these reactions was empirically determined as a difference value between the heat transfer rate to the ablating model (q_{ab}) and the sum of the endothermic thermal parameters (q_a and q_g) previously computed. Numerical results based on this method of treatment were:

Specimen	Rate of Heat Absorption by Heats of Chemical Reactions and Phase Changes (q_p)
Y-31	509 Btu/ft^2-sec
Y-32	576 Btu/ft^2-sec
Y-33	384 Btu/ft^2-sec

The significance of the heats of reaction and phase changes of organic ablating materials is apparent from the above data. Thermal energy expended by this composite protective mechanism was a substantial portion of the incident heat input. In fact, it accounted for 36 to 54 percent of the heat transferred (hot-wall flux) to the stagnation region of the models.

Since (q_p) is a difference value the numerical values obtained are dependent upon the accuracy of the other previously computed heat transfer parameters.

Summary of Heat Transfer Parameters

Numerical results of the heat transfer parameters involved in quasi-steady-state ablation at the stagnation point of the plastic models are graphically presented in Figure 21, and summarized in Table I. Data show that the principle mechanisms of heat absorption and dissipation by the ablating plastic models in air plasma were radiant emission, mass transfer cooling (boundary layer shielding), and latent heats of chemical reactions

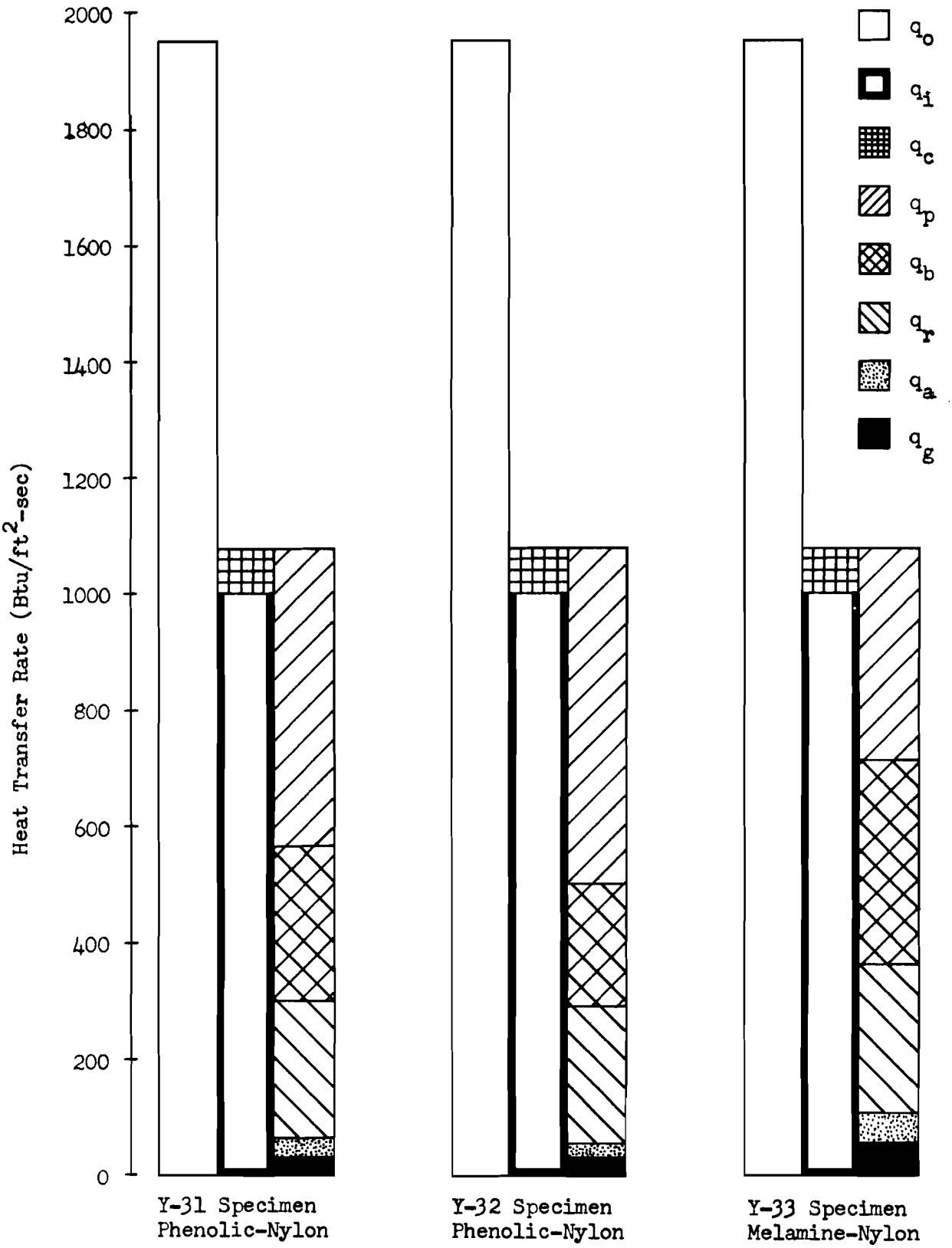

Figure 21. Heat Balance for Several Ablating Plastic Materials

TABLE I

HEAT TRANSFER PARAMETERS FOR STAGNATION POINT STEADY-STATE ABLATION OF SEVERAL PLASTIC MATERIALS

Heat Transfer Parameter	Symbol	Calculated Values (Btu/ft^2-sec)		
		Y-31 Specimen Phenolic - Nylon	Y-32 Specimen Phenolic-Nylon	Y-33 Specimen Melamine-Nylon
Rate of initial heat input (cold-wall flux)	q_o	1950	1950	1950
Rate of heat input at temperature (hot-wall flux)	q_i	1000	1000	1000
Heat flux generated by chemical oxidative reactions	q_c	75	75	75
Rate of heat absorption by chemical reactions and physical transformations	q_p	509	576	384
Rate of heat dissipation by mass transfer cooling (boundary layer shielding)	q_b	265	206	347
Radiant emission flux	q_r	240	240	240
Rate of sensible heat absorption by solid body	q_a	30	25	43
Rate of sensible heat absorption by pyrolytic gases in char substrate	q_g	31	28	61

and physical transformations. The contributions of the sensible heat of the solid body and pyrolytic gases effusing through the char layer were minor.

Heat of Ablation

Experimental data on steady-state ablation of plastic materials have shown a linear relationship between the ablation rate at the stagnation point and the rate of heat input to a non-ablating model at the ablative surface temperature. Under these conditions, a heat balance equation may be written as:

$$q_s = Q^* \rho_b \dot{x} \quad . \tag{15}$$

Where:

q_s = rate of heat transfer to the stagnation point of a non-reacting impermeable wall at the ablative surface temperature (hot-wall flux)
Q^* = effective heat of ablation
ρ_b = density of solid body
$\dot{x}$ = linear ablation rate at the stagnation point.

By transposing the terms in equation (15), and redefining the ablation rate in terms of a mass loss rate $\dot{m}$, we have:

$$Q^* = q_s/\dot{m} \quad . \tag{16}$$

The heat of ablation value, then, expresses the ability of a material to absorb and dissipate heat per unit mass expended. It is an engineering approximation of the ablative performance for a specified hyperthermal environment.

A secondary heat of ablation value reported in the literature, but of lesser importance, is given as:

$$Q = (q_o)_s/\dot{m} \quad . \tag{17}$$

Where:

Q = apparent heat of ablation
$(q_o)_s$ = cold-wall heat transfer rate at the stagnation point
$\dot{m}$ = mass ablation rate.

This ablation value has very limited utility, since the relationship between the mass ablation rate and the cold-wall heat transfer rate is very likely not linear for many materials in the requisite test environments. The popularity of this apparent heat of ablation value is attributed to the high accuracy and ease of determining the cold-wall heat transfer rate of the test environment.

Experimental heat of ablation values were determined for the stagnation point of the three plastic specimens. The effective heat of ablation values were:

Specimen	Effective Heat of Ablation (Q^*)
Y-31	19,600 Btu/lb
Y-32	24,900 Btu/lb
Y-33	15,000 Btu/lb

and the apparent heat of ablation values were:

Specimen	Apparent Heat of Ablation (Q)
Y-31	38,200 Btu/lb
Y-32	48,600 Btu/lb
Y-33	29,300 Btu/lb

For the test conditions under consideration, it took more thermal energy to ablate one pound of Y-32 phenolic-nylon material than was required to ablate a similar amount of the other two test materials.

SECTION IX

DISCUSSION

The heat transfer rate to the model apex region was not uniform throughout the exposure period because of configurational changes. Increased blunting of the specimen apex during hyperthermal exposure effectively lowered the incident thermal flux rate. The magnitude of this effect is presently unknown, but is believed to be within ten percent of the initial flux. In future testing, it may be desirable to enlarge the hemispherical apex region of the models to partially alleviate this condition.

Mass ablation values reported herein may be slightly high due to post-exposure reactions in the hot thermally degraded surface regions of the models. A portion of the heat contained in the char layer was conducted into the interior of the body, and additional volatiles may have been released. Attempts to alleviate this problem by fluid (gases or liquids) quenching were not entirely satisfactory, since thermal shocking was severe enough in certain instances to cause mechanical failure and removal of surface material. In this investigation, the air column from the plasma generator was continued after arc extinction to rapidly cool the hot models.

The ablative performance of a plastic material should be expressed in terms of both mass and linear dimensional changes, and the respective model position being considered. Failure to do so may result in erroneous conclusions concerning the comparative performance of various materials. For example, the order of performance of the test materials on the basis of

total mass loss was: Y-33 melamine-nylon, Y-32 phenolic-nylon, and Y-31 phenolic-nylon, in that order of increasing ablation rates. Different comparative ablation values were obtained, however, from a consideration of the mass and linear ablation rates at the stagnation point of the models. For this case, the order of increasing ablation rates was: Y-32 phenolic-nylon, Y-31 phenolic-nylon and Y-33 melamine-nylon.

The average total mass ablation rate of the Y-32 phenolic-nylon specimen was experimentally determined to be only 2.27 grams per second for the test conditions considered herein. This value compared very favorably with other reference ablation materials evaluated in an identical test environment. Typical comparative values were as follows: ATJ-graphite, 0.7 gm/sec; phenolic-refrasil, 2.5 gm/sec; phenolic-asbestos, 3.0 gm/sec; and nylon molding compound, 3.4 gm/sec.

The linear ablation rate of the Y-32 phenolic-nylon specimen was also relatively low, at a value of 0.004 inch per second. Comparative ablation rates for other materials tested in an identical environment were: ATJ-graphite, 0.003 in/sec; phenolic-asbestos, 0.010 in/sec; phenyl silane-glass, 0.010 in/sec; and nylon molding compound, 0.032 in/sec.

The destructive heat of the environment was confined to the surface region of the plastic models during exposure, with very limited penetration of heat beneath the exposed surface. Since the high temperatures were restricted to a thin thermal thickness layer by the low conductivity of the material, the substrate plastic must have remained at a near-room temperature. It may be inferred, then, that the substrate material has potential load-bearing capability even though the exposed surface is subjected to very high temperatures.

The amount of carbonaceous material formed on the specimens during exposure depends, to some degree, on the type of organic resin in the original material. From an examination of the experimental data, it was noted that the Y-32 phenolic-nylon specimen had an original carbon content 35 percent higher than that of the Y-33 melamine-nylon specimen, yet retained four times as much char material on its surface during exposure. A partial explanation for these results may be associated with the thermal degradative characteristics of the two resinous materials. Phenolic resin with its high initial carbon content underwent uniform coking, which together with the decomposed nylon fabric formed a dense char layer. On the contrary the melamine resin may have been rapidly volatilized leaving behind little residual carbon. Furthermore, this residual carbon may have been weakly bonded together and easily removed from the exposed model by the shear forces of the plasma stream.

The density of the char layer on the various test specimens varied significantly. Average char densities for the Y-31, Y-32, and Y-33 specimens were 0.44 gm/cc, 0.39 gm/cc, and 0.19 gm/cc, respectively. It is interesting to note, however, that the density of the char layer did not vary significantly with respect to the position on a test model.

Spalling of solid material from an ablating surface was apparently due to the formation of gases in the substrate. These gases may have been

trapped locally in pockets by surface resin that hardens and shrinks in response to heating, or by the presence of impermeable reinforcing agents. Under such conditions, gas pressure will tend to increase in the substrate until spalling or catastrophic failure occurs. The importance of forming a porous char layer to permit uniform flow of pyrolytic gases to the surface during hyperthermal exposure should be readily apparent.

The effect of reinforcement orientation on heat penetration into the substrate was shown to be minor for total organic composites. The Y-31 specimen, with its reinforcement axis at the apex parallel to the gas stream, experienced only slightly greater penetration of heat into the body. This was evidenced by comparing the thickness of the volatile-loss region of the individual specimens. The results obtained are in contrast to organic resins reinforced with vitreous fibers. In the latter materials, there is significantly greater heat penetration in the direction of the fiber orientation because of the large difference in thermal conductivity of the organic resin and the inorganic reinforcement.

SECTION X

CONCLUSIONS

A simplified thermal analysis of several ablative plastic materials in an air plasma environment has been presented. Numerical values of the heat absorptive and dissipative parameters of ablation were calculated, and conclusions based on this work were as follows:

Mass transfer cooling (boundary layer shielding), radiant emission and latent heats of chemical reactions and phase transformations were principal mechanisms of heat absorption and dissipation for the materials and environment considered. Contribution of the sensible heat of the solid body and gaseous products in the char layer to heat absorption were minor, and may be neglected in similar thermal analyses of ablative plastic materials.

Mass injection of gaseous products into the boundary layer effectively shielded the exposed specimen from a significant portion of the incident heat flux. This thermal protective mechanism dissipated about one-fourth of the incident environmental heat flux for the test materials and conditions used.

Radiant emission from the hot ablating model was also appreciable during exposure, due to the presence of an environment-generated carbonaceous surface material. The highly emissive surface at a temperature of 5,000°F provided for significant radiant cooling, with a one-fourth dissipation of the incident thermal flux.

Appreciable heat absorption took place during interaction of the material with its environment, as a result of numerous chemical

reactions and phase transformations. Thermal energy expended by these processes were estimated to be about one-third to one-half of the incident flux to the models.

The development of experimental procedures for determining directly individual latent heats of chemical reactions and phase transformations of composite plastic materials will aid significantly in the accurate thermal analysis of ablative materials.

Certain additional conclusions were formulated from the descriptive information and physical measurements of the plastic models during and after air plasma exposure. They were as follows:

The low thermal conductivity of the organic plastic models resulted in low internal heat penetration during exposure. Virtually all of the destructive environmental heat was concentrated within a thin thermal thickness char layer, which varied between 0.02 inch and 0.16 inch for the materials studied.

Orientation of the reinforcement in the organic specimens was not of prime importance in minimizing the attrition rate and heat penetration into the substrate of the models. Apparently, the thermal properties of the resin and reinforcement were too similar to induce significant effects. This type of performance is unlike that previously obtained with organic resins reinforced with vitreous fibers, and evaluated in the same test environment.

The coking characteristic of the phenolic resin was superior to that of the melamine resin. A higher percentage of residual surface carbon with greater strength and density was obtained on test specimens containing phenolic resin.

Since the melamine resin decomposed during exposure to a large fraction of gases with little residual carbon, it may be a suitable resin impregnant for porous refractory materials intended for transpiration cooling systems.

The results of this investigation indicate that the principal mechanisms of heat absorption and dissipation, i.e., boundary layer shielding, radiant emission and latent heats of chemical reactions and phase transformations should be investigated in greater detail to:

a. Provide for accurate calculation of these thermal parameters in terms of the materials and environmental variables involved.

b. Determine the maximum potential of each heat protective mechanism as functions of materials and environmental variables.

c. Indicate means for optimizing ablative materials compositions and constructions.

The criteria of materials performance in a hyperthermal environment involve a consideration of mass and linear changes, internal temperature penetration, structural integrity, heat of ablation value and similar factors. Attempts to express performance in terms of a single materials characteristic or property, such as effective heat of ablation, may lead to erroneous conclusions.

APPENDIX I

LIST OF SYMBOLS

Symbol	Definition	Value
Btu	British thermal unit	
c	specific heat	Btu/lb-^{o}F
cc	cubic centimeter	
C	local velocity gradient of the gas stream	dimensionless
du/dx	velocity gradient of stream	sec^{-1}
d	diffusion coefficient	
D	nose diameter of model	ft
e	emissivity	dimensionless
ft	feet	
g	gravitational constant	32.2 ft/sec/sec
gm	gram	
h	heat transfer coefficient	Btu/ft^2-sec ^{o}R
H	enthalpy per unit mass	Btu/lb
in	inch	
J	heat equivalent of work	778.2 ft-lb per Btu
k	thermal conductivity	Btu-ft/ft^2-sec ^{o}R
l	liter	
L	Lewis number $L = dpc_p/k$	dimensionless
lb	pound	

$\dot{m}$	mass ablation rate	lb/ft^2-sec
M	molecular weight	dimensionless
$\underline{M}$	Mach number, ratio of gas velocity to the velocity of sound at temperature	dimensionless
Nu	Nusselts number Nu $= \bar{q}x/k\ \Delta t$	dimensionless
p	density	lb/ft^3
p_r	Prandtl number, $p_r = \bar{c}_p \mu/k$	dimensionless
P	pressure	atmospheres
q	a specific heat flux	Btu/ft^2-sec
q_a	rate of sensible heat absorption by the solid body in raising its temperature	Btu/ft^2-sec
q_{ab}	heat transfer rate to ablating model neglecting radiation emission and mass transfer cooling	Btu/ft^2-sec
q_b	mass transfer cooling by gas injection into the boundary layer	Btu/ft^2-sec
q_c	heat transfer rate due to exothermic chemical reactions in the boundary layer, at the wall, and within the hot substrate	Btu/ft^2-sec
q_i	hot-wall heat transfer rate with no mass transfer	Btu/ft^2-sec
q_g	heat absorption rate due to sensible heat of gaseous products effusing through the char layer	Btu/ft^2-sec
q_o	cold-wall heat transfer rate	Btu/ft^2-sec
q_p	heat absorption rate by chemical reactions and physical transformations, such as depolymerization, fusion, pyrolysis, vaporization, sublimation, etc.	Btu/ft^2-sec
q_r	radiation emission rate from surface	Btu/ft^2-sec
q_s	stagnation point heat transfer rate with no mass transfer	Btu/ft^2-sec

Q	apparent heat of ablation	Btu/lb
Q^*	effective heat of ablation	Btu/lb
r	radius of hemispherical model	feet
R	undissociated gas constant	0.08205 l-atm/gm-mol-^oK or 52.3 lbs_f-ft^3/lb mol-^oR
Re	Reynolds number $Re = pu\bar{x}/\mu$	dimensionless
sec	second	
t	unit of temperature	
T	unit of time	seconds
u	velocity of stream	ft/sec
V	volume of gas	ft^3
W	weight of gas	lbs
w	wall or surface	
x	total linear dimensions	ft
$\dot{x}$	stagnation point linear ablation rate normal to surface	ft/sec
$\bar{x}$	distance along meridian profile	
Z	Compressibility factor, ratio of the number of moles to original number of moles of diatomic air	dimensionless
γ	Ratio of specific heats of gas, c_p/c_v	dimensionless
υ	kinematic viscosity	ft^2/sec
σ	Stefan-Boltzmann constant	4.806×10^{-13} Btu/ft^2/sec-$^oR^4$
μ	absolute or dynamic viscosity	lb_m/ft/sec

Subscripts

a	air

at	atomic weight of partially dissociated air
b	solid body
c	char layer
D	fraction of energy due to dissociation, or average atomic dissociation energy times the atom mass fraction
f	force
g	gases of pyrolysis
imp	impervious carbon
m	mass
o	free-stream value
p	constant pressure
s	stagnation point value
v	constant volume
w	wall or surface value
l	physically removed from the surface

APPENDIX II

MATERIALS DESCRIPTION AND FABRICATION PROCEDURES

I. Test Materials

Identification			
Composite Type	Phenolic-nylon	Phenolic-nylon	Melamine-nylon
Materials Laboratory Code Number	Y-31	Y-32	Y-33
Supplier	Narmco, Inc.	Formica Corp.	Formica Corp.
Trade Designation	Experimental	Y-25	Experimental 487
Composition and Construction			
Resin Type and Percentage	Phenolic-33%	Phenolic-53%	Melamine-50%
Reinforcement Type and Percentage	Square weave nylon-67%	Square weave nylon-47%	Square weave nylon-50%
Physical Orientation of Reinforcement	Laminar, perpendicular to base	Random, 0.5 inch squares	Random, 0.5 inch squares
Density	63.9 lbs/ft^3	73.0 lbs/ft^3	79.5 lbs/ft^3

II. Fabrication

The organic resin was used as a prepreg on nylon cloth reinforcement. Moldings were fabricated from the impregnated material chopped into 0.5 inch squares and compression molded into cylindrical blocks. The laminar specimen was fabricated from three individually cured laminates. Three sections were press cured at 50 psi and 350°F for two hours, and subsequently bonded together at the following conditions. Fabrication and post-cure conditions were as follows:

Fabrication Conditions			
Maximum temperature	350°F (177°C)	320°F (160°C)	306°F (105°C)
Pressure	50 psi	2200 psi	2750 psi
Duration	6 hours	35 minutes	15 minutes
Post-Cure Conditions			
Temperature	None	284°F (140°C)	221°F (105°C)
Duration	"	48 hours	64 hours

APPENDIX III

STAGNATION POINT HEAT TRANSFER

Method I

Heat transfer to the stagnation point of a hemisphere cylinder from a boundary layer in thermochemical equilibrium may be estimated with reasonable accuracy by using a simple correlation formula:

$$q_s = 0.76/p_r^{0.6} \, (p\mu)_w^{0.1} \, (p\mu)_s^{0.4} \, (H_s - H_w) \, (du/d\bar{x})_s^{0.5} \left[1 + (L^{0.52} - 1) \, (H_D/H_s)\right] . \quad (18)$$

For boundary layer conditions involving a Prandtl number of 0.71 and a Lewis number of unity, equation (18) reduces to:

$$q_s = 0.94 \, (p\mu)_w^{0.1} \, (p\mu)_s^{0.4} \, (H_s - H_w) \, (du/d\bar{x})_s^{0.5} . \quad (19)$$

By numerically solving equation (19), the stagnation point heat transfer rate was obtained for the test conditions under consideration. Specific details of the method of calculation and the origin of the required property values are given below.

Wall and stagnation enthalpy values were determined from the relations:

$$H_w = (c_p)_w \, (t_w - t_b) \quad (20)$$

and

$$H_s = H_o + \frac{u_o^2}{2 g J} \quad (21)$$

where

$$H_o = (c_p)_o \, (t_o - t_w) . \quad (22)$$

Specific heat values for air at t_w and t_o were obtained from references (27) and (28) respectively.

Density of air at t_w was determined from values given by Hilsenrath et al. (27). The density of air at dissociation temperatures was unavailable in the literature, therefore, the values were computed using the ideal gas law relation:

$$p_s = \frac{P_s M_{at} Z}{R\, t_s} \quad . \tag{23}$$

Where:

$$t_s = t_o + \frac{u_o^2}{2\,(c_p)_o g\, J} \quad . \tag{24}$$

Z values for dissociated air were given in reference (29), and viscosity values were obtained from reference (28).

Stagnation point velocity gradient for incompressible potential flow about the hemispherical model was computed using a relation given in reference (30):

$$(du/d\bar{x})_s = 2.6\ u/D \quad . \tag{25}$$

An alternate solution of the local velocity gradient at the stagnation point for modified Newtonian flow may be given as:

$$(du/d\bar{x})_s = \frac{1}{r}\sqrt{\frac{2(P_s - P_o)\, g}{p_s}} \tag{26}$$

in reference (12).

Substituting the appropriate values into equation (19), we arrive at a stagnation point heat transfer rate of 716 Btu/ft^2-sec for the non-ablating model.

Method II

Method II presents an alternate procedure for numerically computing the heat transfer rate to the forward stagnation point of the experimental models. The solution presented is a simplified heat transfer equation previously derived by Reshotko and Cohen (7), and given as:

$$q_s = \frac{k_w\,(t_o - t_w)}{\sqrt{\upsilon_w}} \left(\frac{Nu}{\sqrt{Re_w}}\right)\left(\sqrt{C}\right) \quad . \tag{27}$$

Specific details of the method of calculation and the origin of the required property values are given below.

Free stream and ablation wall temperatures were determined experimentally, and the results may be used directly in equation (27). The effective thermal conductivity of air at t_w was approximated from data given by Greifinger (28), and the kinematic viscosity at t_w was determined from the relation:

$$\upsilon_w = \left(\frac{\mu}{\rho}\right)_w \quad . \tag{28}$$

The dynamic viscosity term was taken from reference (28) data, and the mass density at t_w was computed using the ideal gas law:

$$\rho_w = \frac{P_w M}{R\, t_w} \quad . \tag{29}$$

Reference (29) may also be used for obtaining the mass density value at t_w since the temperature is below that of nitrogen dissociation. Equilibrium properties of air at nitrogen dissociation temperatures may be obtained from references (31) and (32).

The dimensionless heat transfer parameter $Nu/\sqrt{Re_w}$ was chosen from Figure 1 in reference (7), based on test conditions involving axially symmetric flow, Prandtl number of 0.71, and a wall to free-stream ratio of 0.335.

The local velocity gradient at the stagnation point was determined for uniform subsonic potential flow using the following relation:

$$C = \frac{3u_o}{2\,r} \left(1 - 0.252\, \underline{M}_o^{\,2} - 0.0175\, \underline{M}_o^{\,4}\right) \quad , \tag{30}$$

where:

$$\underline{M}_o = \frac{u_o}{\sqrt{\gamma_g R\, t_o}} \quad . \tag{31}$$

All of the necessary relations have been now stated, and may be numerically solved by using experimentally determined and computed fluid property values for the test conditions under consideration. Following this procedure, a heat transfer rate of 1000 Btu/ft^2-sec was obtained for the experimental non-ablating models.

APPENDIX IV

BIBLIOGRAPHY

1. C. Gasley, "Heat Transfer Aspects of the Atmospheric Re-entry of Long-Range Ballistic Missiles," Rand Report R-273, 1 August 1954.

2. I. Gruntfest and L. Shenker, "Behavior of Reinforced Plastics at Very High Temperatures," Modern Plastics 35, pp. 155-163, June, 1958.

3. I. Gruntfest, L. Shenker and V. Saffire, "Behavior of Reinforced Plastics at Very High Temperatures - Part 2," Modern Plastics 36, pp. 137-148, 204, April, 1959.

4. G. Peterson and D. Schmidt, "A Critical Review of Methods for Determining Properties of Reinforced Plastics at Elevated Temperatures," Fifteenth Annual Technical Conference-Volume V, Society of Plastic Engineers, Inc., pp. 64-1 to 64-13, January, 1959.

5. J. Bonin, "Determination of Factors Governing Selection and Application of Materials for Ablation Cooling of Hypervelocity Vehicles," WADC TR 59-87, Chicago Midway Laboratories, March, 1959.

6. M. Sibulkin, "Heat Transfer Near the Forward Stagnation Point of a Body of Revolution," J. Aero. Sc. 19, pp. 570-571, August, 1952.

7. E. Reshotko and C. Cohen, "Heat Transfer at the Forward Stagnation Point of Blunt Bodies," NACA TN 3513, July, 1955.

8. L. Lees, "Laminar Heat Transfer Over Blunt-Nosed Bodies at Hypersonic Flight Speeds," Jet Propulsion 26, pp. 259-269, 274, April, 1956.

9. M. Romig, "Stagnation Point Heat Transfer for Hypersonic Flow," Jet Propulsion 26, pp. 1098-1100, December, 1956.

10. N. Kemp and F. Riddell, "Heat Transfer to Satellite Vehicles Re-entering the Atmosphere," Jet Propulsion, pp. 132-137, 147, February, 1957.

11. P. Rose and W. Stark, "Stagnation Point Heat Transfer Measurement in Dissociated Air," Avco Research Report 3, April, 1957.

12. J. Fay and F. Riddell, "Theory of Stagnation Point Heat Transfer in Dissociated Air," J. Aero Sc. (25) 2, pp. 73-86, February, 1958.

13. H. Kaeppeler and G. Baumann, "Irreversible Stochastic Thermodynamics and the Transport Phenomena in a Reacting Plasma," AFOSR TR 57-20, November 1956.

14. C. Hansen, "Approximations for the Thermodynamic and Transport Properties of High-Temperature Air," NACA TN 4150, March, 1958.

15. C. Cohen, R. Bromberg and R. Lipkis, "Boundary Layers with Chemical Reactions Due to Mass Addition," Jet Propulsion, October, 1958, pp. 659-668.

16. R. Bromberg and R. Lipkis, "Heat Transfer in Boundary Layers with Chemical Reactions Due to Mass Addition," Jet Propulsion, October, 1958, pp. 668-674.

17. S. Scala, "Hypersonic Stagnation Point Heat Transfer to Surfaces Having Finite Catalytic Efficiency," General Electric MOSD Report R58SD236, January, 1958.

18. S. Georgiev, H. Hidalgo and M. Adams, "On Ablation for the Recovery of Satellites," Avco Research Report 47, 6 March 1959.

19. J. Baron, "The Binary-Mixture Boundary Layer Associated with Mass Transfer Cooling at High Speeds," Naval Supersonic Laboratory, Massachusetts Institute of Technology TR 160, May, 1956.

20. L. Roberts, "Mass Transfer Cooling Near the Stagnation Point," NACA TN 4391, September, 1958.

21. H. Bethe and M. Adams, "A Theory for the Ablation of Glassy Materials," Avco Research Report 38, November, 1958.

22. S. Madorsky and S. Straus, "Thermal Degradation of Polymers at Temperatures Up to 850°C," WADC TR 59-64, March, 1959.

23. R. Mixer and C. Marynowski, "A Study of the Mechanism of Ablation of Reinforced Plastics," WADC TR 59-668, Part I, Stanford Research Institute, October, 1959.

24. J. Gordon, "Thermodynamics of High-Temperature Gas Mixtures, and Application to Combustion Problems," WADC TR 57-33, January, 1957.

25. C. Doyle, "Evaluation of Experimental Polymers," WADC TR 59-136, April, 1959.

26. L. Feigenbutz, G. Stiehl and E. Katz, "Combustion Charts for High Energy Fuels - Thermodynamic Properties of Combustion Products," Convair Report ZR-600-001, 21 April 1958.

27. J. Hilsenrath, C. Beckett, W. Benedict, L. Fano, H. Hoge, J. Masi, R. Nuttall, Y. Touloukian, and H. Woolley, "Tables of Thermal Properties of Gases," NBS Circular 564, 1 November 1955.

28. P. Grefinger, "Transport Coefficients of Dissociating and Slightly Ionizing Air," Rand RM 1794, 9 April 1957.

29. W. Moeckel and K. Weston, "Composition and Thermodynamic Properties of Air in Chemical Equilibrium," NACA TN 4265, April, 1958.

30. I. Korobkin and K. Gruenewald, "Investigation of Local Laminar Heat Transfer on a Hemisphere for Supersonic Mach Numbers at Low Rates of Heat Flux," J. Aero. Sc., March, 1957, pp. 188-194.

31. F. Gilmore, "Equilibrium Composition and Thermodynamic Properties of Air to 24,000°K," Rand RM 1543, 1955.

32. J. Hilsenrath and C. Beckett, "Tables of Thermodynamic Properties of Argon-Free Air to 15,000°K," AEDC TN 56-12, 1956.